# How enhancers regulate wavelike gene expression patterns: Novel enhancer prediction and live reporter systems identify an enhancer associated with the arrest of pair-rule waves in the short-germ beetle *Tribolium*

Christine Mau[1], Heike Rudolf[1], Frederic Strobl[2], Benjamin Schmid[3], Timo Regensburger[1], Ralf Palmisano[3], Ernst Stelzer[2], Leila Taher[4*], Ezzat El-Sherif[1*]

[1] Division of Developmental Biology, Department of Biology, Friedrich-Alexander-Universität Erlangen-Nürnberg, 91058 Erlangen, Germany.

[2] Buchmann Institute for Molecular Life Sciences (BMLS), Goethe-Universität Frankfurt Am Main, Frankfurt am Main, Germany.

[3] Optical Imaging Centre Erlangen (OICE), Friedrich-Alexander-Universität Erlangen-Nürnberg, 91058 Erlangen, Germany.

[4] Institute of Biomedical Informatics, Graz University of Technology, A-8010 Graz, Austria.

* Corresponding Authors: Ezzat El-Sherif (ezzat.elsherif@fau.de), Leila Taher (leila.taher@tugraz.at)

## Abstract

A key problem in development is to understand how genes turn on or off at the right place and right time during embryogenesis. Such decisions are made by non-coding sequences called 'enhancers'. Much of our models of how enhancers work rely on the assumption that genes are activated *de novo* as stable domains across embryonic tissues. Such view has been strengthened by the intensive landmark studies of the early patterning of the anterior-posterior (AP) axis of the *Drosophila* embryo, where indeed gene expression domains seem to arise more or less stably. However, careful analysis of gene expressions in other model systems (including the AP patterning in vertebrates and short-germ insects like the beetle *Tribolium castaneum*) painted a different, very dynamic view of gene regulation, where genes are oftentimes expressed in a wavelike fashion. How such gene expression waves are mediated at the enhancer level is so far unclear. Here we establish the AP patterning of the short-germ beetle *Tribolium* as a model system to study dynamic and temporal pattern formation at the enhancer level. To that end, we established an enhancer prediction system in *Tribolium* based on time- and tissue-specific ATAC-seq and an enhancer live reporter system based on MS2 tagging. Using this experimental framework, we discovered several *Tribolium* enhancers, and assessed the spatiotemporal activities of some of them in live embryos. We found our data consistent with a model in which the timing of gene expression during embryonic pattern formation is mediated by a balancing act between enhancers that induce rapid changes in gene expressions (that we call 'dynamic enhancers') and enhancers that stabilizes gene expressions (that we call 'static enhancers').

## Introduction

While an embryo is growing, each cell continuously receives inputs from surrounding cells. The cell processes these inputs and decides its fate accordingly. This decision-making process relies on non-coding sequences called 'enhancers' (1,2). Much of our models of how enhancers work during development relies on the assumption that genes are activated *de novo* across embryonic tissues as stable domains of gene expression (3–5), that then undergo little or no change, either indefinitely or until they do their job whereafter they gradually fade away. Such a view has been strengthened by the intensive landmark studies of the early patterning of the anterior-posterior (AP) axis of the fruit fly *Drosophila melanogaster* embryo, where indeed gene expression domains seem to arise more or less stably (reviewed in (6–9)). However, careful analysis of gene expressions in other model systems painted a different, very dynamic view of gene regulation (9,10). For example, during the AP patterning of vertebrates, oscillatory waves of gene expressions were shown to sweep the embryo before they stabilize into their final positions (9,11–16), demarcating future vertebrae. Likewise, Hox gene expressions propagate along the AP axis of vertebrates, demarcating future axial identities (9,17–21). In both neural tube and limb bud of vertebrates, gene expressions arise in a temporal sequence and spread across the tissue, dividing them into different embryonic fates (22–27).

Surprisingly, patterning of the AP axis of insects, the same process that popularized the static view of gene regulation, turned out to be much more dynamic than previously thought. In insects, the AP axis is divided into segments via the striped expression of a group of genes called 'pair-rule' genes, and into domains of different axial fates via the expression of a group of genes called 'gap genes' (6,9). In the flour beetle *Tribolium castaneum*, a short-germ insect thought to adopt a more ancestral mode of AP patterning than long-germ insects like *Drosophila*, both pair-rule and gap genes are expressed as dynamic waves that propagate from posterior to anterior (28–32). Similar dynamics seem to be involved in segmentation in other insects and arthropods (33–39). Even pair-rule and gap genes in *Drosophila*, classically thought to be expressed stably, were shown more recently to undergo dynamic (albeit limited) posterior-to-anterior shifts (40–44), a phenomenon that has been suggested to be an evolutionary vestige of outright gene expression waves of the sort observed in *Tribolium* (9,45–48). These observations show that the static view of gene regulation, once popularized by classical studies of AP patterning in *Drosophila*, is inaccurate and that gene regulation is in most cases a dynamic phenomenon. Hence, new models of embryonic pattern formation – and concomitantly, new models of how enhancers work within pattern formation models – are needed.

Some of the authors have recently suggested a model that explains the generation of either periodic or non-periodic waves of gene expressions, termed the 'Speed Regulation' model (**Figure 1A,B**) (9,31,32,45,49). In this model, a morphogen gradient (of a molecular factor we termed the 'speed regulator') modulates the speed of either a molecular clock or a genetic cascade. This scheme was shown (*in silico*) to be able to produce periodic waves in the former case (**Figure 1A**), and non-periodic waves in the latter (**Figure 1B**). The model was shown to be involved in generating pair-rule and gap gene expression waves in the early *Tribolium* embryo (30,31), and consistent with recent findings in vertebrate somitogenesis (50–52). Furthermore, a molecular model, termed the 'Enhancer Switching' model (**Figure 1C,D**), has been suggested as a mechanism for how a morphogen gradient could fine-tune the speed of a clock or a genetic cascade, serving as a molecular realization of the Speed Regulation model (9,31,49). The Enhancer Switching model posits that each patterning gene is simultaneously wired into two gene regulatory networks (GRNs) (**Figure 1C**): (*i*) a dynamic GRN that drives periodic or sequential gene activities, and (*ii*) a static GRN that stabilizes gene expressions. The concentration of the speed regulator (shown in gray in **Figure 1C**) activates the dynamic GRN while represses the static GRN, and hence sets

the balance between the contribution of each GRN to the overall dynamics and, consequently, the speed of gene regulation (9,31,49). At high concentrations of the speed regulator, the dynamic GRN is more dominant than the static one, and hence fast oscillations or sequential gene activities are mediated. On the other hand, at low concentrations of the speed regulator, the static GRN is more dominant, and hence slow oscillations or sequential gene activities are mediated. As mentioned, the model posits that each gene is wired into two different GRNs, a requirement that was suggested to be realized using two enhancers per patterning gene: (*i*) a dynamic enhancer that encodes the wiring of the gene within the dynamic GRN, and (*ii*) a static enhancer that encodes the wiring of the gene within the static GRN (**Figure 1D**). The model is partially supported (or rather inspired) by observations in the early *Drosophila* embryo, where the gap gene *Krüppel* (*Kr*) was shown to be regulated by two enhancers whose activities resemble those predicted by the Enhancer Switching model (31,41). Similar observations were made for the *Drosophila* gap gene *giant* (*gt*) (53). Furthermore, in vertebrates, it has been suggested that some enhancers or genetic programs mediate the initiation of segmentation clock waves posteriorly, and others mediate their anterior expressions (54–56).

Most of enhancers regulating AP patterning have been discovered and characterized in *Drosophila*, and so early patterning of the *Drosophila* embryo might seem like a good model system to study enhancer regulation of dynamic gene expressions (57,58). However, the observed gene expression dynamics of *Drosophila* gap and pair-rule genes are only vestigial, not outright waves of the sort observed during the AP patterning of vertebrates or short-germ insects like *Tribolium*. Hence, we sought to test the predictions of our Enhancer Switching model in a system where 'canonical' gene expression waves are observed. We thought that the AP patterning of *Tribolium* serves our purpose well, and more generally, is an excellent model system to study enhancer regulation of dynamic gene expressions. First, *Tribolium* exhibits robust systemic RNAi, which greatly eases the generation of RNAi knockdowns using parental RNAi (59–62). Second, AP patterning takes place in the early *Tribolium* embryo, which eases the interpretation of RNAi knockdowns generated using parental RNAi, without the need of time-specific or tissue-specific genetic perturbations. Indeed, most genetic interactions between gap and pair-rule genes in *Tribolium* have been elucidated by a handful of labs over a few years since the discovery of the efficacy of parental RNAi in *Tribolium* (31,32,63–74). Third, several genetic and genomic tools have been developed for *Tribolium* (75): transgenesis (76,77), transposon-based random mutagenesis (78), large-scale RNAi screens (62), CRISPR-Cas9 (79,80), live imaging (29,81–83), and a tissue culture assay (29,84). Fourth, the *Tribolium* genome is compact compared to vertebrate model systems, rendering enhancer discovery more tractable in that organism.

Thus, in this work, we sought to establish the patterning of the early *Tribolium* embryo as a model system for studying enhancer regulation of dynamic gene expressions and wavelike gene expression patterns. To that end, we set to (*i*) discover enhancer regions that regulate early patterning genes in *Tribolium*, and (*ii*) characterize the spatiotemporal activity dynamics of these enhancers.

Several strategies can be used to predict enhancer regions, each with their own advantages and disadvantages. Assaying open chromatin is a popular method. In particular, "Assay for Transposase-Accessible Chromatin with high-throughput sequencing" (ATAC-seq) (85) is fast and sensitive, and requires very little embryonic tissue (often one embryo, or even a tissue dissected from one embryo) compared to other open chromatin assays. Nevertheless, not all open chromatin regions are active enhancers. Chromatin is also accessible at promoters, insulators, and regions bound by repressors (86–89), and hence, enhancer discovery using open chromatin assays has a high false positive rate. Interestingly, chromatin accessibility has been shown to be dynamic across space and time at active developmental

enhancers compared to other regulatory elements like promoters (90–92), and therefore, dynamic chromatin accessibility has been proposed as an accurate predictor for active enhancers. Thus, in this paper, we used a time-specific and tissue-specific ATAC-seq assay to elucidate the dynamics of open chromatin in space and time in the early *Tribolium* embryos, used the assay to discover a number of active *Tribolium* enhancers, and assessed the association between differential ATAC-seq peak accessibility and enhancer activity.

The second step to understand how enhancers mediate dynamic gene expressions and wavelike gene expression patterns is to characterize the spatiotemporal dynamics driven by the discovered enhancers. *In situ* staining of carefully staged embryos can go a long way in characterizing dynamic gene expressions. However, salient features of these dynamics can be missed using this method, and a strategy to visualize enhancer activities in live embryos is thus needed. Using fluorescent proteins (FP) as reporters for enhancer activities has been traditionally the method of choice in live imaging studies. Nonetheless, FPs suffer from low degradation rates, which results in averaging out of fast changing gene expressions, rendering them unsuitable for visualizing highly dynamic gene activities. This problem can be circumvented by using a destabilized version of FPs (93). However, the reported reduction in FP, although decent, is not enough to detect fast dynamics of many developmental genes. Moreover, destabilized FP suffers from low fluorescent intensity (94). Another strategy is to tag RNAs (95), like in MS2 tagging (96), where MS2 tandem repeats are inserted within a reporter gene. Upon reporter gene activation, the MS2 repeats are transcribed into stem loops that readily bind MS2 virus coat protein (MCP). If MCP-FP fusion proteins are ubiquitously present in the background, they are then recruited at the transcription site in as many numbers as RNA polymerases are actively transcribing the MS2 reporter gene, offering a natural form of signal amplification. This strategy can be used to visualize *de novo* transcription (41,42,97–99), avoiding the averaging effect of using FPs as reporters. Therefore, to study the dynamics of gene expression waves during embryogenesis, we established an MS2-tagging system in *Tribolium*, and used it to visualize the activities of some of the enhancers we discovered using our enhancer discovery system.

In summary, we established in this paper a framework for enhancer discovery and enhancer activity visualization in both fixed and live embryos in *Tribolium*. First, we assayed the dynamics of open chromatin in space and time in the *Tribolium* embryo using ATAC-seq, and used the assay to discover a number of active enhancers. Of importance to future efforts in that vein, we found that active enhancer regions overlap with chromatin accessible sites that significantly vary across the AP axis of the embryo. Second, we established an MS2-MCP enhancer reporter system in *Tribolium* to visualize the activity dynamics of discovered enhancers in both fixed and live embryos. Using this enhancer reporter system, we showed that some of the discovered enhancers regulating gap and pair-rule genes feature expression patterns that are in line with the Enhancer Switching model.

# Results

### Profiling chromatin accessibility landscape along the AP axis of the early *Tribolium* embryo

Genomic regions of increased chromatin accessibility are typically endowed with regulatory activity (92,100). At enhancers in particular, chromatin accessibility has been shown to be dynamic across space and time, and so we set to assay the dynamics of the accessible chromatin landscape in the *Tribolium* embryo. To that end, we dissected the *Tribolium* embryo at the germband stage into three regions across its AP axis (**Figure 2A**): anterior ('a'), middle ('m'), and posterior ('p'), and performed ATAC-seq on each region. We did that for two time points: 23-26 hours after egg lay (AEL) (hereafter, termed IT23), and 26-29 hours AEL (hereafter, termed IT26) (**Materials and Methods**). Our experimental design included six sample groups (3 regions x 2 time points) with 2-3 biological replicates. We generated and sequenced 17

170 ATAC-seq libraries to an average depth of 1,835,762 unique, high-quality pairs of reads (3.6X genomic
171 coverage, **Materials and Methods**). Biological replicates of our ATAC-seq libraries were highly similar with
172 a median Spearman's correlation coefficient of 0.875 (**Supplementary Figure 1**), demonstrating the
173 reproducibility of the data.

174 We identified a total of 12,069 chromatin accessible sites (**Materials and Methods**), with 4,017 being
175 specific to one or two particular regions of the germband and 1,610 to a given time point (**Supplementary**
176 **Figure 2**). In agreement with the ability of ATAC-seq to detect distal regulatory elements in the genome
177 (85), a large proportion of these sites were intergenic or intronic (46%, **Supplementary Figure 3**). Principal
178 component analysis (PCA) of most variable accessible sites (**Materials and Methods**) mainly separated
179 the samples along the AP axis of the embryo (**Figure 2B-D**), where the first principal component (PC1)
180 accounted for 45.3% of the variance, whereas PC2 (18.0% of the variance) predominantly distinguished
181 the middle of the germband from its anterior and posterior ends. Among all 12,069 sites, 3,106 (26% of
182 the accessible genome) were differentially accessible when compared between different regions along
183 the AP axis and/or time point (**Materials and Methods**). For 1,049 of those sites, changes in accessibility
184 were observed in four or more comparisons, indicating more intricate and, generally, specific patterns of
185 accessibility (**Supplementary Figure 4**). Remarkably, while 62% of the constitutively accessible sites
186 corresponded to promoters and gene bodies, 66% of the differentially accessible sites were intergenic or
187 intronic, and this proportion was even higher (74%) among the differentially accessible sites with more
188 specific patterns of accessibility (**Figure 2E**), suggesting that spatiotemporal control of transcription in the
189 early *Tribolium* embryo is largely mediated by enhancers as opposed to promoters. Accessible sites were
190 enriched for binding sites of several transcription factors (**Materials and Methods**; **Supplementary Figure**
191 **5**). In particular, motifs consistent with the binding sites of 20 different transcription factors (Abd-A, Abd-
192 B, Ap, Awh, Cad, CG18599, CG4328, E5, Ems, Eve, Ind, Lab, Lbe, Lbl, Lim3, Pb, PHDP, Pho, Vfl, and Zen)
193 were enriched among all types of sites, independently of their accessibility dynamics.

194 When comparing accessibility along the AP axis at a particular time point, 2,109 sites were differentially
195 accessible, the majority of them along the AP axis at IT26. In addition, only 132 sites were differentially
196 accessible between IT26 and IT23 at the same portion of the embryo (**Supplementary Figure 4B and 4C**).
197 To gain a better insight into the spatial and temporal dynamics of chromatin accessibility, we clustered all
198 differentially accessible sites across the germband regions and time points (**Figure 2F**). Almost half of the
199 sites were either not accessible in the anterior region of the embryo but accessible in the middle and
200 posterior regions (cluster 4,756 sites), or not accessible in the middle and posterior regions of the embryo
201 but accessible in the anterior region (cluster 5,698 sites). Approximately 25% of the sites showed
202 predominantly monotonic changes in accessibility along the AP axis at IT23, either increasing (clusters
203 3,420 sites) or decreasing (cluster 2,347 sites) from the anterior towards the posterior region of the
204 embryo. Fifteen-percent of the sites showed similar accessibility levels in the anterior and middle part of
205 the embryo, and decreased accessibility in the anterior part of the embryo (cluster 6,477 sites). Finally,
206 13% of the sites were most accessible in the middle region of the embryo (cluster 1,408 sites). The sites
207 exhibited similar trends along the AP axis at both time points, although with the exception of the sites in
208 clusters 2 and 4, the sites were generally more accessible at IT26 than at IT23. Functional enrichment
209 analysis of the gene nearest to each site (**Materials and Methods**) revealed that while all clusters are
210 associated with "developmental process" and "anatomical structure development", clusters 1 and 3 are
211 specifically related to "pattern specification process" and "regionalization" and cluster 3 is specifically
212 associated with "anterior/posterior pattern specification" (**Supplementary Figure 6**).

213 Together, our findings indicate that changes in chromatin accessibility in *Tribolium* at this developmental
214 stage are primarily associated with space rather than time, and are particularly evident when comparing
215 the anterior part of the germband to the middle and posterior parts. Furthermore, our data suggests that

sites for which accessibility varies across space are especially likely to be associated with enhancer activity, laying the foundation for a promising enhancer prediction strategy based on differential ATAC-seq peak analysis. Before assessing this proposition, however, we set to establish an enhancer reporter system to validate the activity of predicted enhancers, and analyze their transcriptional dynamics.

**Establishing an MS2-MCP enhancer reporter system to visualize enhancer activity in fixed and live *Tribolium* embryos**

An enhancer reporter system has been previously established in *Tribolium* using *mCherry* as a reporter gene (101). However, long half lives of *mCherry* mRNA and proteins could average out fast transcriptional dynamics, precluding the analysis of gene expression waves. To circumvent this, we created a *Tribolium* enhancer reporter system capable of visualizing *de novo* transcription in both fixed and live embryos. Our enhancer reporter system is composed of the gene *yellow*, which has a long intron (2.7 kb). Visualizing intronic transcription of the reporter gene *yellow* using *in situ* staining in fixed embryos enables the detection of *de novo* transcription, and has been routinely used to analyze fast transcriptional dynamics in enhancer reporter experiments in *Drosophila* (102). To visualize *de novo* transcription in live *Tribolium* embryos, we set to (*i*) modify the *yellow* reporter gene to allow for MS2 tagging, and (*ii*) create a *Tribolium* transgenic line with ubiquitous expression of an MCP-FP fusion. To that end, we created two piggyBac reporter constructs: 'enhancer>MS2-*yellow*' (**Figure 3A**) and 'aTub>MCP-mEmerald' (**Figure 3B**). For the enhancer>MS2-*yellow* construct, we place an enhancer of interest upstream of the *Drosophila* Synthetic Core Promoter (DSCP) and a MS2-*yellow* reporter gene. The MS2-*yellow* reporter is composed of 24 tandem repeats of MS2 stem loops inserted in the 5' UTR of the *yellow* gene, followed by an SV40 poly(A) tail. For the aTub>MCP-mEmerald line, we created a piggyBac construct in which the ubiquitous alpha-tubulin promoter was placed upstream of a nuclear localization sequence (NLS) and an MCP-mEmerald fusion, followed by an SV40 poly(A) tail.

This system is capable of visualizing enhancer activity both in fixed and live embryos. To visualize aggregate enhancer activity in fixed embryos, *yellow* gene expression is visualized using *in situ* staining in embryos carrying the enhancer>MS2-*yellow* construct. To visualize *de novo* transcription in fixed embryos, an *in situ* probe against *yellow* intron is used instead. To visualize *de novo* transcriptional activity of an enhancer in live embryos, a male beetle carrying the enhancer>MS2-*yellow* construct is crossed with a female beetle carrying the aTub>MCP-mEmerald construct. If active, the enhancer should drive the expression of the MS2-*yellow* reporter in the progeny. The transcribed MS2 loops would then recruit aTub>MCP-mEmerald fusion proteins at the transcription site of the reporter gene, enriching the mEmerald fluorescent signal against the weak mEmerald background.

Via piggyBac transgenesis, we successfully generated a transgenic beetle line carrying the MCP-mEmerald construct, in which a ubiquitous mEmerald fluorescence is detected (**Figure 3C**). We then sought to test our enhancer>MS2-*yellow* reporter system, using a previously discovered *Tribolium* enhancer, hbA, that regulates the *Tribolium* gap gene *hunchback* (*hb*) (101). *hb* is expressed in multiple domains in the early *Tribolium* embryo: in the serosa, in an anterior domain, in a secondary posterior domain (shown in orange, blue, and purple, respectively in **Figure 3D**), and in the nervous system (not shown). Enhancer hbA drives the anterior expression of *Tribolium hb* (101) (blue in **Figure 3D**). Via piggyBac transgenesis, we successfully generated a transgenic beetle line carrying the hbA>MS2-*yellow* construct. Examining *yellow* expression using *in situ* hybridization chain reaction (HCR) (103) in early hbA>MS2-*yellow* embryos using both exonic (**Figure 3E,F**) and intronic (**Figure 3F**) probes, we confirmed that the *yellow* expression in hbA>MS2-*yellow* line is similar to the *mCherry* expression in a previously tested hbA>*mCherry* line (101).

260 To test the live imaging capability of our MS2-MCP system, we crossed the hbA>MS2-*yellow* and the
261 aTub>MCP-mEmerald lines. Imaging early embryos of the progeny (hbA>MS2-*yellow* ; aTub>MCP-
262 mEmerald) (**Movie S1; Figure 3G**), we observed weak and diffuse mEmerald signal within the nuclei, and
263 bright puncta at a rate of at most one puncta per nucleus. The bright mEmerald puncta are distributed
264 along the AP axis initially as a cap that eventually refines into a stripe (**Supplementary Figure 9**),
265 resembling the *yellow* expression of the hbA enhancer reporter visualized using *in situ* HCR staining (**Figure**
266 **3E,F**). We conclude, therefore, that such bright mEmerald puncta are mEmerald enrichments at
267 transcribed MS2 loops, reflecting the *de novo* transcription driven by the hbA enhancer. Hence, both
268 individual nuclei of the early *Tribolium* embryo and *de novo* transcription driven by the hbA enhancer can
269 be visualized and detected in a single cross of hbA>MS2-*yellow* line and the MCP-mEmerald line,
270 confirming our success in establishing an MS2-MCP enhancer reporter system that is capable of visualizing
271 enhancer activity in live *Tribolium* embryos.

272

273 **Assessing the association between differential accessibility and enhancer activity**

274 We then sought to use our enhancer reporter system to test putative enhancers suggested by our ATAC-
275 seq analysis. In selecting a set of putative enhancers to test, we restricted our analysis to genomic regions
276 around three genes, all involved in AP patterning in *Tribolium*: the gap genes *hb* (**Figure 4A**) and *Kr*
277 (**Supplementary Figure 7A**) as well as the pair-rule gene *runt (run*) (**Figure 4B)**. Candidate enhancer
278 regions were chosen based on the presence of accessible sites in any region along the AP axis and/or time
279 point (**Materials and Methods**), whether or not they were differentially accessible.

280 Out of nine tested reporters, four successfully drove *yellow* expressions in the early *Tribolium* embryo
281 (**Figure 4C**). While enhancer hbA drove an expression that overlaps with *hb* anterior expression, enhancer
282 hbB drove an expression that overlaps with *hb* expression in the serosa (compare hbA and hbB activities
283 in **Figure 4C**; see **Figure 3D** for the constituents of *hb* expression in *Tribolium*). Enhancer runA drove an
284 expression that partially overlaps the endogenous *run* expression in the nervous system during the late
285 germband stage (runA in **Figure 4C**). Enhancer runB drove a striped expression that overlaps endogenous
286 *run* expression in the ectoderm, but neither the striped *run* expression in the mesoderm, nor the nervous
287 system expression (runB in **Figure 4C**).

288 We then determined whether there is any association between differential accessibility and enhancer
289 activity using our tested enhancer constructs, augmented with previously published *Tribolium* enhancers
290 that regulate the genes *single-minded* (*sim*) and *short gastrulation* (*sog*) (104) (**Supplementary Figure 8**).
291 In total, eleven enhancer constructs were analyzed, where 54.5 % of constructs (six constructs) were
292 active and 45.5 % of constructs were not active (five constructs). We found that five out of six active
293 constructs overlapped differentially accessible sites, while one active construct overlapped a site that was
294 not differentially accessible (**Material and Methods**). Two out of five non-active constructs overlapped
295 sites that were not differentially accessible, while the remaining three overlapped sites that were
296 differentially accessible (**Figure 4D**; see **Supplementary Figure 7** for details). Therefore, about 60% of
297 analyzed differentially accessible sites were associated with active enhancers whereas only 30% of
298 analyzed constitutively accessible sites were associated with active enhancer regions (**Figure 4E**). These
299 results support our hypothesis that differential accessibility is associated with enhancer activity.

300

301

302 **Testing the plausibility of the Enhancer Switching model**

303 Next, we set out to test the plausibility of the Enhancer Switching model by examining the activity
304 dynamics of some of the discovered enhancers. The model predicts that for a gene involved in generating
305 gene expression waves, there exists two enhancers: (*i*) a 'dynamic enhancer' responsible for initiating the
306 wave, and (*ii*) a 'static enhancer' responsible for arresting the wave into a stable gene expression
307 domain(s) (**Figure 1C,D**).

308 Among the discovered enhancers in *Tribolium*, two enhancers are potentially involved in generating gene
309 expression waves: hbA and runB. The expressions driven by both enhancers overlap with the expression
310 waves of their corresponding genes: enhancer runB with the periodic waves of the pair-rule gene *run*, and
311 enhancer hbA with the non-periodic wave of the gap gene *hb*. To test if the spatiotemporal dynamics
312 driven by these enhancers conform with some of the predictions of the Enhancer Switching model, we
313 first ran simulations of the model and used them to carefully analyze model predictions. Then, we used
314 our enhancer reporter system to track the enhancer activity dynamics of runB and hbA in space and time
315 using *in situ* HCR staining in carefully staged fixed embryos as well as using our MS2-MCP system in live
316 *Tribolium* embryos. Finally, we compared our model predictions with the observed enhancer activity
317 dynamics.

318 <u>Careful examination of the predictions of the Enhancer Switching model</u>

319 To carefully analyze the predictions of the Enhancer Switching model in space and time, we ran a
320 simulation (**Movie S2**) of a 3-genes realization of the periodic version of the model (**Figure 1C**, where an
321 oscillator is used as a dynamic module). Carefully analyzing model outputs for total activity of constituent
322 genes, static enhancer reporters, and dynamic enhancer reporters revealed two characteristics of the
323 spatiotemporal dynamics of their activities (**Figure 5A**). First, endogenous genes and reporters of their
324 dynamic and static enhancers are all expressed in waves that propagate from posterior to anterior (**Figure**
325 **5A**). Second, expressions driven by dynamic enhancers progressively decrease in the posterior-to-anterior
326 direction, matching the progressive decrease of the speed regulator concentration (**Figure 5A**). On the
327 other hand, expressions driven by static enhancers progressively increase in the posterior-to-anterior
328 direction, opposite to the direction of increase of the speed regulator concentration (**Figure 5A**). This is a
329 natural consequence of the activating vs repressing effect of the speed regulator on dynamic vs static
330 enhancers, respectively (**Figure 1C**).

331 However, a minor complication arises when one considers a more realistic instantiation of the Enhancer
332 Switching model. In our simulation of the model presented in **Figure 5A** (and in our simulations presented
333 in previous publications (31,32,45)), we assumed that the stabilized gene expression domains at the
334 anterior remain stable indefinitely (**Figure 5A**). However, we observe experimentally that such stable
335 phase is transient, after which gene expression domains gradually fade (notice the progressive fading of
336 the first *run* stripe after its stabilization at the anterior in **Figure 6A,B**). This effect can be implemented
337 computationally by reducing the strength of the static enhancers (**Figure 5B**, **Movie S3**). In this case, the
338 expression driven by a dynamic enhancer is very similar to the total expression of the gene expression
339 wave: both arise maximally at the posterior and gradually fade as they propagate towards anterior (**Figure**
340 **5B**). On the other hand, the expression wave driven by the static enhancer remains unique, as it, for the
341 most part, increases in the direction of its propagation (until it eventually fades; **Figure 5B**). This means
342 that while it is easy to identify a static enhancer from its enhancer reporter activity, it is not as simple to
343 identify a dynamic enhancer. In particular, an enhancer that drives an expression that arises maximally at

344 the posterior and gradually fades as it propagates towards anterior might be either a dynamic enhancer
345 or simply an enhancer that drives the entirety of the gene expression wave.

346 Examining the activity dynamics of enhancer runB using *in situ* HCR staining

347 To test the predictions of the Enhancer Switching model, we started by examining the spatiotemporal
348 dynamics of one of the primary pair-rule genes, *run*, simultaneously with those of one of its enhancers
349 that we discovered in this study, runB, using HCR in carefully staged embryos (**Figure 6A**). Endogenous *run*
350 expression (green in **Figure 6A**) periodically arises from posterior and gradually propagates towards
351 anterior, forming stable striped expression (that eventually fades). Concomitantly, runB>*yellow* is
352 expressed as well in a periodic wave that propagates from posterior to anterior (red in **Figure 6A**).
353 However, in contrast to endogenous *run* expression, the expression wave of runB>*yellow* appears weakly
354 in the posterior and gradually strengthens as it propagates towards anterior. These observations are in
355 line with the predicted enhancer dynamics of our model, in which runB acts as a static enhancer for *run*.
356 First, runB drives gene expression waves that propagate from posterior to anterior. Second, runB activity
357 progressively increases in the posterior-to-anterior direction, corresponding inversely with the
358 progressive drop of concentration of the Caudal (Cad) gradient (**Figure 6B**), which has been suggested to
359 act as a speed regulator for pair-rule and gap genes in *Tribolium* (30,31), and more generally, an
360 evolutionary conserved posterior determinant in arthropods (along with Wnt) (64,105–108).

361 We notice, however, that the wave dynamics of runB>*yellow* expression are less discernible in posterior
362 germbands (see **Figure 6A**, 23-26 hours AEL). We wondered if this is due to long degradation delays of
363 *yellow* mRNAs. In line with this possibility, we noticed that mature runB>*yellow* stripes at anterior
364 germbands are more stable and long-lived than those of endogenous *run* (**Supplementary Figure 10**). To
365 circumvent this, we examined runB->*yellow* expression using an intronic probe against *yellow*, and indeed
366 found that the intronic expression of runB->*yellow* is both discernible in the posterior germband and in
367 line with endogenous *run* expression anteriorly (**Supplementary Figure 10**). This shows that, indeed,
368 degradation delays of the reporter gene *yellow* is larger than that of endogenous *run*, leading to averaging
369 out of *run* expression wave dynamics, a problem that can be alleviated using intronic *in situ* staining.

370 Examining the activity dynamics of enhancer runB using live imaging

371 To verify that runB indeed drives expression waves that propagate from posterior to anterior, we
372 performed a live imaging analysis of runB activity using our MS2-MCP system in *Tribolium*. Crossing runB
373 enhancer reporter line (runB>MS2-*yellow*) with our aTub>MCP-mEmerlad line, and imaging early embryos
374 of the progeny, we observed bright mEmerald puncta distributed along the AP axis as a stripe (**Movie S4**;
375 **Figure 6C**), an expression that resembles that of *yellow* in the same reporter line visualized using *in situ*
376 HCR staining (compare **Figures 6A and 6C**). To characterize the spatiotemporal activity of runB enhancer,
377 circumventing the ambiguity introduced by nuclear flow, we developed a computational strategy to: (*i*)
378 track the nuclei of the early live *Tribolium* embryo, (*ii*) detect MS2 puncta, and (*iii*) associate the detected
379 MS2 puncta to corresponding nuclei (**Materials and Methods**). Furthermore, to smoothen out the highly
380 stochastic expression of *de novo* transcription, we applied a moving average window to MS2 signal across
381 time to estimate an accumulated activity of the runB enhancer (**Movie S5**; **Materials and Methods**).
382 Tracking the accumulated activity in space, after discounting nuclear flow, revealed that runB indeed
383 drives a wave of activity that progressively increase in strength as it propagates from posterior to anterior
384 (**Movie S6**; **Figure 6D**), fitting the role of a 'static enhancer' within our Enhancer Switching model.

385 Examining the activity dynamics of enhancer hbA using live imaging

386 Gap genes are expressed as well in waves in the *Tribolium* embryo, albeit in a non-periodic fashion. Gap
387 gene waves are initialized by a pulse of *hb* expression that arises in the posterior of the blastoderm at 14
388 hours AEL, that eventually propagates towards anterior, clears from posterior, forming a stripe of *hb*
389 expression at the anterior part of the embryo (**Figure 3D,E**).

390 Similar to our analysis of runB enhancer, we used our MS2-MCP system to estimate the accumulated
391 mRNA signal driven by enhancer hbA, and tracked it in space and time in live *Tribolium* embryos (**Movie**
392 **S7**, **Movie S8**). We found that enhancer hbA drives a wave of activity that propagates from posterior to
393 anterior (**Figure 6E**). In contrast to enhancer runB, however, we found that enhancer hbA drives strong
394 expression in the posterior that weakens as it propagates towards anterior (compare **Figures 6D** and **6E**).
395 As concluded by our simulations of the Enhancer Switching model (**Figure 5B**), this indicates that hbA
396 either drives the entirety of *hb* expression, or acts as a dynamic enhancer within the Enhancer Switching
397 model.

398

399 # Discussion

400 In this paper, we established a framework for enhancer discovery in *Tribolium* using tissue- and time-
401 specific ATAC-seq (**Figure 2**). We showed that differential accessible sites analysis across space and time
402 yields a sizeable increase in enhancer prediction accuracy (**Figure 4**). We also developed an enhancer
403 reporter system in *Tribolium* able to visualize dynamic transcriptional activities in both fixed and live
404 embryos (**Figure 3**). Both our enhancer discovery and activity visualization systems are efforts to establish
405 the AP patterning in *Tribolium* as a model system for studying dynamic gene expressions, especially gene
406 expression waves, a phenomenon commonly observed during embryonic development (9,10,109).
407 Although our experimental framework is suitable for exploring how enhancers mediate dynamic gene
408 expression in an unbiased fashion, we set in this work to test the plausibility of a specific model: the
409 'Enhancer Switching' model (**Figure 1**), a scheme some of the authors have recently suggested (31,49) to
410 elucidate how gene expression waves are generated at the molecular level. The model posits that each
411 gene within a genetic clock or a genetic cascade is regulated by two enhancers: one 'dynamic' that induces
412 rapid changes in gene activity, and another 'static' that stabilizes it. By modulating the balance between
413 the potency of dynamic vs static enhancers, the tuning of the speed of gene regulation is achieved (**Figure**
414 **1C,D**). We first characterized the model's predictions for the spatiotemporal activities of enhancer
415 reporters of dynamic and static enhancers (**Figure 5**). The model predicts that reporter constructs of
416 dynamic enhancers would drive a gene expression wave that progressively decreases in intensity in the
417 direction of its propagation, whereas reporter constructs of static enhancers would drive a wave whose
418 intensity increases in the direction of its propagation (**Figure 5A**). We then used our enhancer discovery
419 framework to discover a number of enhancers regulating embryonic patterning in the early *Tribolium*
420 embryo (**Figure 4**). One of these enhancers, runB, drove an expression pattern consistent with a role as a
421 static enhancer for the pair-rule gene *run* (**Figure 6A-D**). Another enhancer, hbA, drove an expression
422 pattern consistent with a role as a dynamic enhancer for the gap gene *hb* (**Figure 6E**). However, the
423 expression pattern driven by hbA could be also interpreted as driving the entirety of *hb* expression (**Figure**
424 **6E**, **Figure 5B**). We present these findings as tentative support for the Enhancer Switching model, whereas
425 a strong support requires: (1) finding enhancer pairs for several gap and pair-rule genes whose activity
426 dynamics match those predicted for static and dynamic enhancers, and (2) verifying that the deletion of
427 either dynamic or static enhancers result in phenotypes predicted by the model (**Figure 7**). Specifically,

deleting a static enhancer should reduce the gene expression wave into an (almost) homogenously oscillating (or sequentially activating) domain at the posterior, that fails to resolve into gene expression bands anteriorly (**Figure 7B**), while deleting a dynamic enhancer should abolish the entire gene expression (**Figure 7C**). Future works should aim at testing these predictions, modifying the model, or finding alternative models.

The long-term goal of establishing the experimental framework presented in this paper is to understand the regulation of dynamic gene expressions at the molecular level. The model system we adopted exhibits, however, very particular kind of dynamics: wave dynamics. This sounds like attempting to solve a fringe problem, since the most notable and well-known instance of this problem has been documented during vertebrate somitogenesis, in which case it is unclear if such wave dynamics are of any functional significance. Indeed, the predominant model of somitogenesis, namely the 'Clock-and-Wavefront', can do without such wave dynamics. Furthermore, gene expression waves observed during somitogenesis are periodic, making the problem even more of a fringe case, as there are far less cases of periodic gene expression patterns in development than non-periodic ones. However, upon reviewing experimental observations in other model systems, one finds strong indications that such wave dynamics, especially in their non-periodic version, are more prevalent than has previously thought, albeit described in varied terminologies. For example, Hox genes, which are expressed in a non-periodic pattern along the AP axis of vertebrates, have been described to 'spread' anteriorly upon their emergence from the posterior (18). Similarly, neural fate-specifying genes have been described to arise in a variable temporal order along the dorsoventral axis of the vertebrate neural tube, and so are effectively expressed as a non-periodic wave (22). Furthermore, the functional importance of such wave dynamics is manifest in embryonic tissues that undergo no or limited elongation during the patterning process, where a pure Clock-and-Wavefront model fails to explain the patterning process (9) (e.g. the vertebrate neural tube and limb bud, the vertebrate embryo at the early phase of somitogenesis (110), and the blastoderm of short-germ insects). Even for elongating tissues that can be patterned by a classical Clock-and-Wavefront mechanism, wave dynamics have been suggested to foster robustness for the patterning process (30,111,112).

As we set our experimental framework as means to study gene expression waves in development, we should note that we have only discussed one type of waves, namely 'kinematic waves' (also called 'phase waves' or 'pseudo-waves') (10,113). A kinematic wave propagates without the need of 'diffusion' or cell-to-cell communication, and gives the appearance of spreading across the tissue due to differences in gene expression timing between different cells. This type of wave can mediated by the Speed Regulation model discussed in this study (**Figure 1A, and 1B**). A wave, however, could be also a 'trigger' wave, which propagates with the help of cell-to-cell communication (10). One key experiment to differentiate between a trigger versus a kinematic wave is to insert a barrier along its path. The barrier should block a trigger wave, while a kinematic wave would appear to continue propagating across the barrier. A barrier experiment of that sort indicated that the periodic gene expression waves observed during somitogenesis are indeed of the kinematic type (11). Another key feature that differentiates a trigger from a kinematic wave is the spatial variability of the wave's wavelength. Kinematic waves of the sort induced by the Speed Regulation model has a key signature: it emanates as wide bands, that progressively shrink in the direction of its propagation, and hence the wave's wavelength is variable across space (**Figure 1A,B**). A trigger wave, on the other hand, is typically of a fixed wavelength. Most of the waves described during embryonic development (including gap and pair-rule waves in *Tribolium*) shrink in the direction of their propagation, and thus exhibit the appearance of kinematic waves (see for example **Figure 6D,E**).

Once a gene expression wave is determined to be kinematic, mechanistically explaining how it is produced reduces to elucidating how the speed of gene regulation can be tuned by a morphogen gradient (according

473 to Speed Regulation model: **Figure 1A,B**). Whereas the phenomenon of gene expression waves is of
474 significance within the domain of embryonic pattern formation, the problem of how to tune the speed of
475 gene regulation has a wider applicability. For example, the temporal progression of different
476 developmental stages is species-dependent and, hence, needs to be tunable by evolution (114), the timing
477 of developmental progression in insects is controllable by the steroid hormone ecdysone (115), and the
478 time needed for progenitor cells to differentiate needs to be tuned to control (relative) population/organ
479 sizes, which furthermore needs to be adjustable by evolution (116–119). Thus, the model problem we are
480 introducing in this paper has wide applicability within and beyond the domain of embryonic pattern
481 formation.

482 In this paper, we considered the Enhancer Switching model as a molecular realization for how to modulate
483 the timing of gene regulation. The central idea behind the model is that tuning the timing of gene
484 regulation is the result of setting the balance between two GRNs (**Figure 1C**): one GRN mediates rapid
485 changes in gene regulation (termed 'dynamic GRN'), and another stabilizes gene expressions (termed
486 'static GRN'). This scheme could be realized by just one enhancer per gene, if such an enhancer is able to
487 switch its wiring depending on the concentration of a graded molecular factor (the speed regulator). The
488 phenomenon of one enhancer exerting multiple functions has indeed been observed and termed
489 'enhancer pleiotropy' (120–124). However, we suggested a molecular strategy that uses a separate
490 enhancer for each wiring scheme (**Figure 1D**) (31). This strategy, we believe, is more molecularly feasible
491 and ensures modularity and evolvability (31). Indeed, the complex regulation of many genes in
492 development are usually undertaken by several enhancers, each encoding simple regulatory logic (125–
493 127).

494 While the evidence for the Enhancer Switching model is still sketchy, parallels (or evolutionary vestiges)
495 to it is evident in *Drosophila*. After an initialization phase, the striped expression of *Drosophila* pair-rule
496 genes stabilizes and undergoes frequency doubling. The switching between the initialization to
497 stabilization mode of pair-rule regulation is mediated by the switch of early to late acting enhancers.
498 Interesting, this switch seems to be mediated by timing factors encoded by two pioneer factors: Zelda and
499 Opa, where Zelda is responsible for activating the early network and Opa for the late network (128–130).
500 Indeed, in *opa* mutants, the frequency doubling of pair-rule genes is lost in *Drosophila* (128). Interestingly,
501 *cad* (potentially along with *zelda*), and *opa* were found to be activated sequentially in the *Drosophila*
502 embryo (and *Nasonia*'s (131)), reflecting a similar sequential activation in space and time in the *Tribolium*
503 embryo (47,132). This gives rise to a possible unified model for early-to-late enhancer switching in insects.
504 In this model, early/posterior expression of AP patterning genes are mediated by early/dynamic
505 enhancers, while late/anterior expressions are mediated by late/static enhancers. This transition is
506 mediated ancestrally by Wnt/Cad gradient, possibly indirectly through Zelda and Opa, where Zelda is
507 responsibly for activating early/posterior/dynamic enhancers, whereas Opa is responsible for activating
508 late/anterior/static enhancers (9). Such late enhancers might, however, play a mere maintaining role as
509 indeed commonly believed, while a static enhancer as suggested by the Enhancer Switching model has a
510 key functional role in sculpting the waves. Such functional importance can only be elucidated using an
511 enhancer deletion experiment (**Figure 7**).

512 Mechanisms for tuning the speed of gene regulation other than the Enhancer Switching model, however,
513 are also possible. For example, histone modifications have been shown to influence the timing of gene
514 activation or repression (133). Although such a mechanism does not offer complete tunability of the speed
515 of gene regulation (since histone modifications usually specifically influence either gene activation or

516 repression), it can explain certain phenomena; for example, controlling the timing of sequential activation
517 (but not inactivation) of fate specifying genes (116,117,133). Modulating enhancer accessibility could be
518 yet another mechanism for tuning the timing of gene regulation (115). However, such a scheme would
519 require a yet unknown mechanism for stably maintaining gene expression while enhancer accessibility is
520 reduced, without the help of a stabilizing enhancer (otherwise, it would be simply an instance of the
521 Enhancer Switching model). Such possibilities could also be explored using our model system, if
522 complemented with genomic assays for histone modifications.

523 In yet another hypothesis for how to generate gene expression waves, the timescale of the genetic process
524 (be it a genetic clock or a cascade) is tuned by modulating protein production time delay or the coupling
525 strength between cells (134–140). However, in *Tribolium*, reactivating the gap gene *hb* all over the embryo
526 resulted in two distinct responses (32): reactivation of the genetic gap cascade in the posterior (where the
527 speed regulator Wnt/Cad has high concentration), whereas the expression of already formed gap gene
528 domains at the anterior is erased. This indicates that the switch in behavior of gap gene regulation
529 between the anterior vs posterior in the early *Tribolium* embryo is not due to a simple change either in
530 protein and transcript degradation rates or cell-to-cell coupling strengths, but due to a difference in the
531 genetic makeup between these two regions, giving more credit to our Enhancer Switching model.

532

## 533 Data Availability

534 ATAC-seq tracks were included in the iBeetleBase Genome Browser (https://ibeetle-base.uni-
535 goettingen.de/genomebrowser/) (141).

536

## 537 Acknowledgement

538 This work is supported by a DFG grant (EL 870/2-1) to EE, and a doctoral fellowship from the German
539 Academic Scholarship Foundation to CM. We thank Rodrigo Nunes da Fonseca, Emilila Esposito, Alexander
540 Aulehla, and Shelby Blythe for providing valuable tips for ATAC-seq library preparation.

541

## 542 Materials and Methods

### 543 Beetle Cultures

544 Beetle cultures were reared on flour supplemented with 5 % dried yeast in a temperature- and humidity-
545 controlled room at 24 °C. To speed up development, beetles were reared at 32 °C.

### 546 PiggyBac Enhancer Reporter Constructs

547 A piggyBac plasmid with the 3 x P3-mCherry/mOrange marker construct and multiple cloning sites (77)
548 was used to generate all enhancer constructs in this study. For enhancer constructs, putative enhancer
549 regions, the *Drosophila* synthetic core promoter (101,142), and the MS2-*yellow* reporter gene (97,99)
550 were amplified by PCR, assembled through ligation, and inserted into the multiple cloning site of the
551 piggyBac plasmid. Used primers are listed in **Table S1**.

552 **Creation of the MCP-mEmerald construct**
553 An artificial sequence, consisting of (i) an AscI restriction enzyme site, (ii) the *Tribolium castaneum*
554 Georgia2 (GA2) background strain-derived (143) tubulin alpha 1-like protein (aTub) promoter (144), (iii) a
555 *Tribolium castaneum* codon-optimized open-reading frame consisting of (a) the SV40-derived nuclear
556 localization signal (NLS) tag (145) coding sequence, (b) the human influenza hemagglutinin (HA) tag (146)
557 coding sequence and (c) the bacteriophage MS2 coat protein (MCP) (147) coding sequence, and (iv) a NotI
558 restriction enzyme site, was *de novo* synthesized and inserted into the PacI/SacI restriction enzyme site
559 pair of pMK-T (Thermo Fisher Scientific) by the manufacturer. The resulting vector was termed
560 pGS[aTub'NLS-HA-MCP]. The sequence was excised with AscI/NotI and inserted into the backbone of the
561 accordingly digested pACOS{#P'#O(LA)-mEmerald} vector (77). The resulting vector was termed
562 pAGOC{aTub'NLS-HA-MCP-mEmerald}, contained (i) an expression cassette for mEmerald-labeled (148)
563 and NLS/HA-tagged MCP, (ii) the piggyBac 3' and 5' inverted terminal repeats (149), as well as (iii)
564 mOrange-based (150) and mCherry-based (151) eye-specific (152) transformation markers, and was co-
565 injected with the standard piggyBac helper plasmid (153) into *Tribolium castaneum* embryos following
566 standard protocols (154,155) to achieve germline transformation.

567 ***Tribolium* Transgenesis**
568 PiggyBac constructs were transformed into vermilion$^{white}$ (156) with mCherry/mOrange as visible makers.
569 Germline transformation was carried out using the piggyBac transposon system (153,157).

570 **Egg Collections for Developmental Time Windows**
571 Developmental time windows of three hours were generated by incubating three hours egg collections at
572 24 °C for the desired length of time. Beetles were reared in flour supplemented with 5% dried yeast.

573 ***In Situ* Hybridization and Imaging of Fixed Embryos**
574 *In situ* hybridization was performed using the third generation *in situ* hybridization chain reaction (HCR)
575 method (103). All probe sets and hairpins were ordered at Molecular Instruments. Lot numbers of probe
576 sets are as follows: PRA978 (*run* mRNA), PRA979 (*hb* mRNA), PRC655 (*yellow* mRNA), and PRE723 (*yellow*
577 intron). Images were taken with a Leica SP5 II confocal. A magnification of 20x or 63x was used at a
578 resolution of 2,048 x 1,024. Images were processed and enhanced for brightness and contrast using Fiji
579 (158).

580 **Live Imaging**
581 aTub>MCP-mEmerlad females were crossed with hbA>MS2-*yellow* or runB>MS2-*yellow* males. Three
582 hours egg collections were generated and incubated for eleven (crossing with hbA) or fourteen hours
583 (crossing with runB) at 24 °C. Embryos were dechorionated by immersion in 1 % bleach for 30 s twice.
584 Embryos were mounted using the hanging drop method and covered with halocarbon oil 700 (Sigma).
585 Time-lapse movies were taken by capturing 41 planes every 3 min over ~ 6 h at 21 °C with a Leica SP5 II
586 confocal. A magnification of 63X was used at a resolution of 1,024 x 900. To produce unprocessed live
587 imaging movies (**Movies S1 and S4**), a maximum Z-projection is applied to the image sequence in Fiji.

588 **Computational Processing and Analysis of Live Imaging Movies**
589 To characterize the transcription dynamics driven by enhancer MS2 enhancer reporters in live embryos,
590 circumventing the ambiguity introduced by nuclear flow, we developed a computational strategy to: (1)
591 segment nuclei, (2) detect MS2 spots and estimate their intensity, (3) associate MS2 spots to nuclei and
592 track nuclei over time, and estimate mRNA intensity.

593 (1) Segmenting nuclei
594 In Fiji, stacks were first maximum intensity projected. Contrast was enhanced using the CLAHE plugin with
595 a block size of 128. Nuclei were then detected as local maxima, disregarding maxima with an intensity
596 below half the image maximum intensity. Detected maxima were used as seed points for the watershed
597 algorithm to retrieve nuclei outlines.

598 (2) MS2 spot detection
599 In Fiji, MS2 spots were detected as local 3D maxima after applying a 3D Difference-of-Gaussians filter. Its
600 parameters, the standard deviations of the Gaussians, tolerance (the minimum intensity difference
601 between neighbor spots, analogous to the ImageJ 'Find Maxima' implementation) and a lower threshold
602 (to disregard spots with low intensity) were set empirically.

603 (3) Tracking nuclei and MS2 spots over time and mRNA estimation
604 We used strategies similar to those described in (41) using Matlab.

605 **ATAC-seq Library Preparation**
606 Embryos of the nGFP line (29) were collected in flour supplemented with 5% dried yeast for 3h and
607 incubated for desired time length at 24 °C. Embryos were dechorionated by immersion in 1 % bleach for
608 30 s twice. Selected embryos were dissected into three parts (anterior, middle, and posterior). For each
609 biological replicate, three of the same embryo parts were pooled, and three replicates were prepared for
610 each sample condition. Library preparation was performed as previously described (159,160).
611 Tagmentation was performed for 8 min. ATAC-seq libraries were sequenced on an Illumina NovaSeq 6000
612 at the Novogene Cambridge Genomic Sequencing Centre. 2x150 bp paired-end Illumina reads were
613 obtained for all sequenced ATAC-seq libraries.

614 **ATAC-seq Data Pre-processing**
615 Sequencing reads were trimmed with cutadapt (161) with parameters "-u 15 -U 15 -q 30 -m 35 --max-n 0
616 -e 0.10 -a CTGTCTCTTATA -A CTGTCTCTTATA" to remove adapter sequences and mapped to the *Tribolium*
617 *castaneum* reference genome (Tcas5.2, GCA_000002335.3) with BWA-MEM (version 0.7.12-r1039 (162).
618 Next, read duplicates were marked with Picard MarkDuplicates (version 2.15.0, Picard Toolkit. 2019.
619 Broad Institute, GitHub Repository. https://broadinstitute.github.io/picard/; Broad Institute.). Low quality
620 and duplicated reads were filtered using samtools view (version 1.10, (163)) with parameters "-F 1804 -f
621 2 -q 30". To flag regions that appear to be artifacts, we generated a blacklist using a strategy similar to the
622 one developed by the ENCODE Project (164). Specifically, the genome was first divided into non-
623 overlapping 50bp bins. Next, the BAM files containing the filtered mapped reads were converted into
624 BigWig files using BAMscale (version 1.0, (165)) with parameters "scale --operation unscaled --binsize 20
625 --frag". Using the resulting BigWig files, the mean signal for each bin was computed across all sequencing
626 libraries. Finally, bins with a mean signal equal to or greater than 100 were flagged as artifacts and
627 included in a "blacklist". The threshold was determined by visual inspection of the distribution of the mean
628 signals. Reads mapping to genomic regions in the blacklist were filtered out using samtools view (version
629 1.7, (163)) with parameters "-L" and "-U".

630 Peaks were called on individual replicates using macs3 (v3.0.0a7, https://github.com/taoliu/MACS; (166))
631 callpeak with parameters "-g 152413475 -q 0.01 -f BAMPE". The sets of peaks called in each sample were
632 then compared to each other and merged if they overlapped by at least 1 bp. Only merged peaks
633 supported by peaks called in at least two different samples and on scaffolds assigned to linkage groups

634 were considered for subsequent analyses. These peaks are further referred to as the set of "all"
635 (consensus) chromatin accessible sites.

636 Chromatin accessible sites were annotated with HOMER (version 4.11.1, (167)) using the
637 annotatePeaks.pl function.
638

639 **Genomic tracks**
640 Normalized ATAC-seq coverage tracks were generated with BAMscale (version 1.0, (165)) using
641 parameters "scale --frag --binsize 20 --smoothen 2". The tracks of different biological replicates of the
642 same sample were then merged with the UCSC tools bigWigMerge and bedGraphToBigWig
643 (http://hgdownload.cse.ucsc.edu/admin/exe/linux.x86_64/), and visualized with pyGenomeTracks
644 (version 3.7, (168,169)).

645 **Differential Accessibility Analysis**
646 Differential accessibility analysis of the sites between different regions of the germband and/or time
647 points was performed using the edgeR (version 3.36.0, (170)) and DESeq2 (version 1.34.0, (171)) methods
648 within the DiffBind (version 3.4.11, (172),
649 http://bioconductor.org/packages/release/bioc/vignettes/DiffBind/inst/doc/DiffBind.pdf). Peaks with a
650 false discovery rate (FDR) less than or equal to 0.05 for edgeR and/or DESeq were considered significant.
651 Read counts for each peak were quantified with the dba.count() function, with parameters
652 "score=DBA_SCORE_TMM_MINUS_FULL, fragmentSize=171, bRemoveDuplicates=TRUE". Briefly, this
653 normalizes the read counts using Trimmed Mean of M-values (TMM, (173)) scaled by the full library size.
654 We further refer to these values as "accessibility scores". Sites that had a mean accessibility score larger
655 than the median and a standard deviation larger than the 3rd quartile were defined as the "most variable
656 accessible sites".

657 Clustering
658 The z-score normalized accessibility scores of the differentially accessible sites were clustered using k-
659 means (with k=6) as implemented in the kmeans() R function. The function was executed with default
660 parameters except for "nstart=1000", which initializes the algorithm with 1000 different sets of random
661 centers and settles for those giving the best fit.

662 Complete linkage on the pairwise Pearson correlation distances (1-Pearson correlation coefficient) was
663 performed with the hclust() R function to hierarchically cluster the differentially accessible sites based on
664 their average accessibility scores across the replicates of each sample group. The pheatmap (version
665 1.0.12, Raivo Kolde (2019). pheatmap: Pretty Heatmaps. R package version
666 1.0.12. https://CRAN.R-project.org/package=pheatmap) R package was used for visualization using row-
667 scaling.

668 Functional analysis
669 Functional enrichment analysis was carried out with the PANTHER API. Specifically, the "statistical
670 enrichment test" tool was used with the "GO Biological Process complete" *Tribolium castaneum* database.
671 Overrepresented GO terms/pathways were determined using default parameters (Fisher's exact test,
672 False Discovery Rate (FDR) < 0.05). All the positive overrepresented GO biological process (BP) terms were
673 considered. The API was last accessed on August, 2022.

674 Motif analysis
675 Motif enrichment analysis was carried out using XSTREME with default parameters except for "--streme-
676 totallength 4000000 --meme-searchsize 100000 --ctrim 500 --streme-nmotifs 5" (version 5.4.0, (174)).
677 Motifs discovered *de novo* were compared to the motifs in the insects JASPAR 2022 CORE non-redundant
678 database (175) to identify putative transcriptional regulators. Sequences in which soft-masked
679 nucleotides comprised 95% or more were not considered for the analysis.

680 Overlap between Differentially Accessible Sites and Constructs
681 A construct was considered to be overlapping with a site if at least 90% of the site overlapped with the
682 construct.

683 **Computational Modeling**
684 For the Enhancer Switching Models, we used computational algorithms described in (31,32,49), using
685 the Matlab programs provided in these publications with minor modifications.

686

687 # Figure legends

688 **Figure 1. The Enhancer Switching Model as a molecular realization of the Speed Regulation Model.** (**A**)
689 The Speed Regulation Model for periodic patterning. Left: Cells can oscillate between two states mediated
690 by a molecular clock: high (shown in dark blue), and low (shown in light blue). The concentration of the
691 speed regulator (shown in gray) modulates the speed of the molecular clock (i.e. its frequency). Right: A
692 gradient of the speed regulator across a tissue (represented by a row of cells) induces a periodic wave
693 that propagates from the high to the low end of the gradient. (**B**) The Speed Regulation Model for non-
694 periodic patterning. Same as for the periodic case (A), except the molecular clock is replaced with a genetic
695 cascade that mediates the sequential activation of cellular states (represented by different colors). (**C**) The
696 Enhancer Switching Model, a molecular realization of the Speed Regulation model, is composed of two
697 GRNs: one dynamic and one static. The dynamic GRN can be either a clock (to mediate periodic patterning)
698 or a genetic cascade (to mediate non-periodic patterning). The static GRN is a multi-stable gene circuit
699 that mediates the stabilization of gene expression patterns. The speed regulator activates the dynamic
700 GRN but represses the static GRN, and so a gradient of the speed regulator (shown in gray) mediates a
701 gradual switch from the dynamic to the static GRN along the gradient. Shown example realizations of
702 dynamic and static GRNs, where the dynamic GRN represents either a molecular clock or a genetic
703 cascade, depending on the absence or presence of the repressive interaction shown in yellow,
704 respectively. (**D**) Separate dynamic and static enhancers encode the wiring of each gene (shown here only
705 for the red gene) within the dynamic and static GRNs, respectively.

706

707 **Figure 2. Chromatin accessibility dynamics during AP patterning of the early *Tribolium* embryo.** (**A**)
708 Embryos 23-26 h AEL (IT23) or 26-29 h AEL (IT26) were dissected and cut into anterior (a), middle (m), and
709 posterior (p) part. Left: nGFP embryo in the eggshell. Right: dissected and cut nGFP embryo. (**B**) Principal
710 component analysis (PCA) on the accessibility scores of the most highly accessible and variable sites in the
711 dataset. PCA was performed using the PCA() function in the "FactoMineR" R package with default
712 parameters. Only the first two principal components (PC) of the data are represented. The first PC explains
713 45.3% of the variance in the data, the second PC, 18.0%. (**C**, **D**) Boxplots showing the scores of PC1 and
714 PC2 by space (C) and time (D). The thick line indicates the median (2nd quartile), while the box represents
715 interquartile range (IQR, 1st to 3rd quartiles). Outliers are shown as dots. (**E**) Genomic annotation of

716 different classes of chromatin accessible sites: all (consensus) sites, constitutive sites (i.e., consensus sites
717 that are not differentially accessible), all differentially accessible sites, and most specifically accessible
718 sites (i.e., sites differentially accessible in four or more comparisons). (**F**) K-means clustering of
719 accessibility scores for differentially accessible sites. Accessibility scores have been z-score scaled for each
720 site.

721

722 **Figure 3. An MS2-MCP enhancer reporter system to visualize enhancer activity in fixed and live**
723 ***Tribolium* embryos tested using the *Tribolium hb* enhancer hbA.** (**A**) Our enhancer reporter construct:
724 An enhancer of interest is placed upstream of a DSCP, followed by 24 tandem repeats of MS2 stem loops,
725 the gene *yellow*, then an SV40 poly(A) tail. **(B)** The aTub>MCP-mEmerald construct: ubiquitous alpha-
726 tubulin promoter was placed upstream of an NLS and an MCP-mEmerald fusion, followed by an SV40
727 poly(A) tail. (**C**) Overview image of an aTub>MCP-mEmerald embryo at the germband stage. (**D**) A
728 schematic showing *hb* expression in *Tribolium*. In the early blastoderm, *hb* is expressed in the serosa
729 (orange) and as a cap in the posterior half of the embryo (blue) (T1) that eventually resolves into an
730 expression band in the anterior (blue in T2 and T3). Later during the germband stage (T4), the anterior
731 expression (blue) fades and a new *hb* expression arises in the posterior (purple). (**E**) Spatiotemporal
732 dynamics of endogenous *hb* (green) and reporter gene *yellow* (red) expressions in hbA->*yellow Tribolium*
733 embryos. Left panel: Time-staged embryos from 14 to 26 h AEL at 24 °C, in which mRNA transcripts (*hb*:
734 green, *yellow*: red) were visualized using *in situ* HCR staining. Nuclear staining (Hoechst) is in gray. Right
735 panel: Fluorescence signal along the dorsal-ventral axis was summed up to generate intensity distribution
736 plots along the AP axis. (**F**) Detection of *de novo* transcription via *in situ* HCR staining of intronic *yellow*.
737 Nuclear staining (Hoechst): blue; exonic *yellow* (*yellow* mRNA): red; intronic *yellow*: purple. Embryo
738 outline shown in dashed line. (**G**) Live imaging snapshot of a hbA>MS2-*yellow* ; aTub>MCP-mEmerlad
739 *Tribolium* embryo. Diffuse mEmerald signal is observed in nuclei (outlined in white dashed line). mEmerald
740 fluorescence is enriched at transcription sites (bright puncta: MS2-MCP signal). In all embryos shown:
741 posterior to the right.

742

743 **Figure 4. Correlation of enhancer activity with differential accessibility.** (**A, B**) The ATAC profiles (two
744 time points (IT23, IT26) with three embryo regions (a, m, p) per time point) for *hb* (A) and *run* (B). Tested
745 enhancer regions at these loci are shown as boxes underneath the ATAC profiles. Differential accessible
746 sites match well with active enhancer regions (purple boxes; red box: not active enhancer construct).
747 ATAC tracks were created with pyGenomeTracks. (**C**) Enhancer reporter constructs for active enhancer
748 regions shown in (A) and (B), in which mRNA transcripts were visualized using *in situ* HCR staining
749 (endogenous gene expression: green, reporter gene expression: red, merge: yellow). Nuclear staining
750 (Hoechst) is in gray. hbA drives reporter gene expression in a stripe (embryo in germband stage shown).
751 hbB drives reporter gene expression in the serosa (embryo in blastoderm stage shown). runA drives
752 reporter gene expression in a subset of the endogenous *run* CNS expression (embryo in late germband
753 stage shown). runB drives reporter gene expression in stripes outside of the most posterior part of the
754 embryo (embryo in germband stage shown). Posterior to the right. (**D**) The correlation between
755 differential accessibility and construct activity was determined. Eleven enhancer constructs were
756 analyzed: 54.5 % of constructs (six constructs) were active and 45.5 % of constructs were not active (five
757 constructs). Five out of six active constructs are associated with sites that are differentially accessible,
758 while one active construct overlaps with a site that is not differentially accessible. Two out of five not
759 active constructs match sites that are not differentially accessible, while the remaining three not active
760 constructs are associated with sites that are differentially accessible (see Supplementary Figure 7 for

details). (**E**) Enhancer prediction efficiency of our enhancer prediction method based on differential peak analysis. Same enhancer constructs were analyzed as in (D). About 60 % of analyzed differential peaks were associated with active enhancer construct regions whereas in about 40 % of analyzed cases differential peaks could be found at not active enhancer construct regions. In contrast, about 70 % of analyzed non-differential peaks were associated with not active enhancer construct regions. About 30 % of analyzed non-differential peaks are associated with active enhancer construct regions.

**Figure 5. Simulation of the Enhancer Switching model with different static enhancer strengths.** Shown simulation outputs of the Enhancer Switching model for a reporter gene driven by dynamic (yellow) or static (black) enhancers, as well as an endogenous gene driven by both dynamic and static enhancer (green). Two versions of the model were simulated and contrasted: with strong (A) vs weak (B) static enhancer activity. (**A**) Model simulation with strong static enhancer activity. Each wave of the endogenous gene expression follows first the dynamics of the dynamic enhancer and switches along space (in the tapering direction of the speed regulator, shown in gray) and time to the dynamics of the static enhancer to form a stable expression domain. (**B**) Model simulation with a weaker static enhancer: dynamic enhancer activity resembles endogenous gene expression pattern. Left panels: spatial plots across time. Right panels: Kymographs.

**Figure 6. Analysis of enhancer activity dynamics using the MS2-MCP live imaging system.** (**A**) Shown are spatiotemporal dynamics of endogenous *run* (green) and the reporter gene *yellow* (red) expression in runB->*yellow* embryos. Left panel: Time-staged embryos from 14 to 26 h AEL at 24 °C, in which mRNA transcripts (*run*: green, *yellow*: red) were visualized using *in situ* HCR staining. Nuclear staining (Hoechst) is in gray. Right panel: Intensity distribution plots along the AP axis. Both *run* and runB->*yellow* are expressed in waves that propagate from posterior to anterior. runB->*yellow* expression wave, however, starts weak posteriorly and progressively increases in strength as it propagates towards anterior, until it eventually overlaps with the stabilized *run* stripes anteriorly. (**B**) Left panel: *in situ* HCR staining for endogenous *run* (green) and reporter gene *yellow* expression (red) combined with antibody staining for Cad proteins (purple) in a runB->*yellow* blastoderm embryo (upper row) and a runB->*yellow* germband embryos (lower row). Nuclear staining (Hoechst) is in gray. Right panel: Intensity distribution plots along the AP axis for *yellow* expression in a whole *Tribolium* blastoderm (upper panel), and within the region indicated in dashed yellow in a *Tribolium* germband. Cad forms a posterior-to-anterior gradient in both balstoderm and germband embryos. runB activity increases progressively as Cad concentration drops towards anterior. (**C**) Live imaging snapshot of a runB>MS2-*yellow* ; aTub>MCP-mEmerlad *Tribolium* embryo. Diffuse mEmerald signal is observed in nuclei. mEmerald fluorescence is enriched at transcription sites (bright puncta: MS2-MCP signal). Left panel: original snap shot; Middle: nuclei that exhibit MS2-MCP signal are outlined in white circles; Right: A close up to nuclei with MS2-MCP signal. (**D, E**) Tracking estimated mRNA activity driven by runB **(D)** and hbA **(E)**. Left panels (in both (D) and (E)): Snapshots across time from live embryo movies in which nuclei (shown in gray) are tracked and MS2 signals are averaged over time (using a moving average filter with a length of 10 movie frames) to estimate mRNA activity (shown in red). Middle panel: Intensity distribution plots along space for representative images in left panel. Right panel: A kymograph showing estimated mRNA activities of enhancer reporters across space and time. In all embryos shown: posterior to the right.

**Figure 7. Simulation of the Enhancer Switching Model with deleted enhancers.** Shown simulation outputs of the Enhancer Switching model under three experimental conditions: **(A)** an intact locus, **(B)** a locus in which the static enhancer is deleted, and **(C)** a locus in which the dynamic enhancer is deleted.

**Movie S1. MS2 live imaging of hbA enhancer reporter**. Live imaging of a "hbA>MS2-*yellow* ; aTub>MCP-mEmerlad" *Tribolium* embryo during the blastoderm stage. NLS signal within the aTub>MCP-mEmerald construct mediates a weak and diffuse mEmerald signal within nuclei. Upon transcription, MS2 loops within the hbA>MS2-*yellow* construct recruit MCP-mEmerald fusion proteins at transcription sites, resulting in mEmerald bright puncta. Here bright mEmerald puncta are observed throughout the posterior end of the blastoderm, reflecting transcriptional activity of enhancer hbA in the early *Tribolium* embryo. Posterior to the right.

**Movie S2. Simulation of the Enhancer Switching Model with strong static enhancer activity.** Shown are outputs of a computer simulation of the Enhancer Switching model with strong static enhancer activity. Activity dynamics of reporter genes driven by the dynamic and static enhancers are shown in yellow and black, respectively. Activity dynamics of endogenous gene expression driven by both the dynamic and static enhancers are shown in green. Speed regulator gradient is shown in grey.

**Movie S3. Simulation of the Enhancer Switching Model with weak static enhancer activity.** Shown are outputs of a computer simulation of the Enhancer Switching model with wea static enhancer activity. Activity dynamics of reporter genes driven by the dynamic and static enhancers are shown in yellow and black, respectively. Activity dynamics of endogenous gene expression driven by both the dynamic and static enhancers are shown in green. Speed regulator gradient is shown in grey.

**Movie S4. MS2 live imaging of runB enhancer reporter**. Live imaging of a "runB>MS2-*yellow* ; aTub>MCP-mEmerlad" *Tribolium* embryo during the blastoderm stage. NLS signal within the aTub>MCP-mEmerald construct mediates a weak and diffuse mEmerald signal within nuclei. Upon transcription, MS2 loops within the runB>MS2-*yellow* construct recruit MCP-mEmerald fusion proteins at transcription sites, resulting in mEmerald bright puncta. Here bright mEmerald puncta are observed initially to be distributed as a posterior cap that eventually propagates towards anterior to form a stable band. Posterior to the right.

**Movie S5. Estimated mRNA transcription driven by enhancer runB in the early *Tribolium* embryo.** Shown is a live imaging movie of a "runB>MS2-*yellow* ; aTub>MCP-mEmerlad" embryo (same as in Movie S4) computationally processed to show an estimation of accumulated mRNA abundance driven by enhancer runB (red) as well as MS2-mEmerald signal (reflecting *de novo* transcription; green). Posterior to the right.

**Movie S6. Plots of estimated mRNA transcription dynamics driven by enhancer runB across space and time.** Shown is a dorsoventral projection of a tracked spatiotemporal activity of enhancer runB (same embryo as in **Movies S4,S5**). Horizontal axis: AP axis; posterior to the right.

844

845 **Movie S7. Estimated mRNA transcription driven by enhancer hbA in the early *Tribolium* embryo.** Shown
846 is a live imaging movie of a "hbA>MS2-*yellow* ; aTub>MCP-mEmerlad" embryo (same as in Movie S1)
847 computationally processed to show an estimation of accumulated mRNA abundance driven by enhancer
848 hbA (red) as well as MS2-mEmerald signal (reflecting *de novo* transcription; green). Posterior to the right.

849

850 **Movie S8. Plots of estimated mRNA transcription dynamics driven by enhancer hbA across space and**
851 **time.** Shown is a dorsoventral projection of a tracked spatiotemporal activity of enhancer hbA (same
852 embryo as in **Movies S1,S7**). Horizontal axis: AP axis; posterior to the right.

853

854 **Supplementary Figure 1. Correlation between ATAC-seq sequencing libraries**. Mapped sequencing reads
855 of each biological replicate were used to calculate correlation between pairs of replicates. The values
856 represent the Pearson correlation coefficients between pairs of sequencing libraries.

857

858 **Supplementary Figure 2. Upset plot comparing the number of sites identified in samples corresponding**
859 **to IT23 and IT26 as well as along the AP axis**. (**A**) Plot corresponding to IT23 and IT26. (**B**) Plot
860 corresponding to samples along the AP axis (a, m, and p). The number of sites in each of the sets
861 considered is represented by the width of the bars in the bar chart at the bottom left. Each bar in the bar
862 chart at the top represents the number of sites in an intersection. The intersection is indicated by filled
863 circles below each bar. Note that the intersection sets are disjoint.

864

865 **Supplementary Figure 3. Annotation of consensus sites**. A total of 12069 consensus sites were analyzed.
866 Consensus sites overlap with promoter-TSS (22.3 %), TSS (8.5 %), exons (23.5 %), introns (30.2 %), and
867 intergenic regions (15.5 %), respectively. TSS: Transcription Start Site.

868

869 **Supplementary Figure 4. Analysis of differentially accessible sites**. (**A**) The accessibility of sites was
870 compared between three different parts of the germband (anterior, middle, and posterior) at two time
871 points (IT23 and IT26). All possible 15 comparisons were considered. A total of 3106 sites were differential
872 accessible. (**B**) For the same part of the embryo, 132 sites were differentially accessible between two time
873 points. (**C**) A total of 2109 sites were differentially accessible between two different parts of the germband
874 at a given time point.

875

876 **Supplementary Figure 5. Motif Analysis.** Enrichment of TF motifs in accessible sites depending on their
877 accessibility (y-axis, see Figure 1D for details). The size of the dots represent the fraction of sequences
878 with one or more motif occurrences. The TFs (if known) are indicated on the x-axis.

879

880 **Supplementary Figure 6. Functional enrichment analysis of the clusters of differentially accessible sites**.
881 Clustering of all differentially accessible sites across the AP axis and time points. All clusters are associated
882 with "developmental process" and "anatomical structure development", while clusters 1 and 3 are

specifically related to “pattern specification process” and “regionalization” and cluster 3 is specifically associated with “anterior/posterior pattern specification”.

**Supplementary Figure 7. Genomic tracks of analyzed enhancer reporter constructs.** Genomic tracks of analyzed enhancer reporter constructs. ATAC profiles (two time points (IT23, IT26) with three embryo regions (a, m, p) per time point) are shown for (**A**) *Kruppel* (*Kr*), (**B**) *short gastrulation* (*sog*), and (**C**) *single-minded* (*sim*). Analyzed enhancer regions at these loci are shown as purple (active enhancer region) or red (not active enhancer region) boxes underneath the ATAC profiles. KrA enh - KrD enh were tested in *Tribolium* in this work. Other enhancer regions were evaluated in a cross-species context in *Drosophila* (104). Differential accessible sites match well with active enhancer region of *sim* (C). No differential accessible site overlap with the previously described active enhancer region of *sog* (B). Not active KrB enh region is not overlapping with differential accessible sites, while overlaps are observed between differential accessible sites and not active KrA enh, KrC enh, and KrD enh regions (A). ATAC tracks were created with pyGenomeTracks.

**Supplementary Figure 8. Simulations with different static enhancer strength.** Computational simulation of reporter gene expression driven by dynamic (yellow) or static enhancer (black), respectively as well as endogenous gene expression (green) driven by both, dynamic and static enhancer. Analyzed was the spatiotemporal pattern of gene expression. (**A**) No static enhancer: dynamic enhancer strength d=3, static enhancer strength c=0 (same as in Figure 7B, deleted static enhancer). Each wave of the endogenous gene expression follows the dynamics of the dynamic enhancer. Due to the lack of static enhancer activity, endogenous gene expression waves fail to stabilize as stable expression domains. (**B**) Very weak static enhancer: d=3, c=0.5. Each wave of the endogenous gene expression follows the dynamics of the dynamic enhancer. Due to very weaker static enhancer activity, dynamic enhancer activity resembles whole gene expression pattern (compare to Figure 5B). Endogenous gene expression waves are impaired in forming stable expression domains. (**C**) Weak static enhancer: d=3; c=1. Dynamics of the endogenous gene expression are mainly governed by dynamic enhancer activity. Weak static enhancer activity stabilizes endogenous gene expression waves as stable expression domains. (**D**) Intermediate strong static enhancer: d=3, c=1.5. Each wave of the endogenous gene expression follows first the dynamics of the dynamic enhancer and switches along space to the dynamics of the intermediate strong static enhancer to form a stable expression domain. Left panel: Intensity plots. The speed regulator is shown in grey. Right panel: Kymographs.

**Supplementary Figure 9. Analysis of hbA enhancer activity on a fixed embryo.** Images of a fixed hbA>MS2-*yellow* ; aTub>MCP-mEmerlad *Tribolium* embryo in the germband stage (upper image: overview; lower image: close-up view of the indicated region in the overview image). The bright mEmerald puncta (MS2-MCP signal at active transcription sites) refine into a stripe resembling the *yellow* expression of the hbA enhancer reporter visualized using *in situ* HCR staining (compare to Figure 3E).

**Supplementary Figure 10. Visualizing runB>yellow expression waves in the germband using exonic vs intronic probes.** runB expression waves resemble more those of endogeneous *run* (shown in green) when visualized using intronic (shown in pruple) in situ probe than exonic (shown in red) probes .

927

928

929

930

931 **Supplementary Table 1: List of used primers.** frw: forward, rev: reverse.

| Description | Sequence (5` - 3`) |
|---|---|
| pBPGUw promoter frw + BsaI into NotI | AAATTTGGTCTCCGGCCGCGATCGAGCGCAGCGGTATAAAA |
| pBPGUw promoter rev + BsaI into BamHI | AAATTTGGTCTCGGATCCGTTTGGTATGCGTCTTGTGATTCAAAG |
| pBPGUw promoter-24xMS2-y frw + HindIII | AAATTTAAGCTTGATCGAGCGCAGCGGTATAAAA |
| pBPGUw promoter-24xMS2-y rev + STOP + SbfI | AAATTTCCTGCAGGTTAACCCACAGAATTTGTAGAGACACTAATACTG |
| DSCP frw + HindIII | AAATTTAAGCTTGATAAACGGCCGGCAGCGGTATAAAAGGG |
| DSCP rev + BsaI into BamHI | AAATTTGGTCTCGGATCCGGGCTGCAGATTGTTTAGCTTGTTCAGC |
| hbA frw + BsaI into XmaI | AAATTTGGTCTCCCCGGGCACCCTATTTACGCAACGGCTATTTTC |
| hbA rev + BsaI into HindIII | AAATTTGGTCTCAAGCTTTGGTGGAGATGTTATGGTATGGTCG |
| hbB frw + XmaI | AAATTTCCCGGGCACCCATTGTGACAGCTCGG |
| hbB rev + HindIII | AAATTTAAGCTTTTCTCTGAGGCATAATCCCACTAATTACC |
| runA frw + XmaI | AAATTTCCCGGGGGGTAGTTGTCGGTTAGATGCAATATTGTG |
| runA rev + HindIII | AAATTTAAGCTTCGTTATTCGGAGGTGTCCATTATTGGAAGG |
| runB frw + XmaI | AAATTTCCCGGGCGCAGCGTTATGAAAAATACGGAACAA |
| runB rev + HindIII | AAATTTAAGCTTCCGCCTAGCGAGCATTAGTGC |
| runC frw + BsaI into XmaI | AAATTTGGTCTCCCCGGGGGCTAACATTTGATTCGCACATCGG |
| runC rev + BsaI into HindIII | AAATTTGGTCTCAAGCTTCCTTGTTCAGCAATCACTCAAATATTGTGC |
| KrA frw + BsaI into XmaI | AAATTTGGTCTCCCCGGGAATAATTCCGAAACGCAAAGAGATAGACCC |
| KrA rev + BsaI into HindIII | AAATTTGGTCTCAAGCTTGTGGCATCAAATGGTAGTGACACATCG |
| KrB frw + BsaI into XmaI | AAATTTGGTCTCCCCGGGGTGGCATCAAGTAGTAGTGAGACATCG |
| KrB rev + BsaI into HindIII | AAATTTGGTCTCAAGCTTCTAACGGTGTAGGGTTTGCATAGCAAA |
| KrC frw + BsaI into XmaI | AAATTTGGTCTCCCCGGGTAATCTGAGGAGGCGACGTCTAGC |
| KrC rev + BsaI into HindIII | AAATTTGGTCTCAAGCTTCGATGTCTCACTACTACTTGATGCCAC |
| KrD frw + BsaI into XmaI | AAATTTGGTCTCCCCGGGTTCCATAGCCGACTTGATGCACAACC |
| KrD rev + BsaI into HindIII | AAATTTGGTCTCAAGCTTGCTAGACGTCGCCTCCTCAGATTC |

932

933

934 ## References


935 1. Spitz F, Furlong EEM. Transcription factors: from enhancer binding to developmental control. Nat
936 Rev Genet. 2012 Sep;13(9):613–626.

937 2. Shlyueva D, Stampfel G, Stark A. Transcriptional enhancers: from properties to genome-wide
938 predictions. Nat Rev Genet. 2014 Apr;15(4):272–286.

939 3. Small S, Blair A, Levine M. Regulation of even-skipped stripe 2 in the Drosophila embryo. EMBO J.
940 1992 Nov;11(11):4047–4057.

941 4. Clyde DE, Corado MSG, Wu X, Paré A, Papatsenko D, Small S. A self-organizing system of
942 repressor gradients establishes segmental complexity in Drosophila. Nature. 2003 Dec
943 18;426(6968):849–853.

944 5. Hoch M, Seifert E, Jäckle H. Gene expression mediated by cis-acting sequences of the Krüppel
945 gene in response to the Drosophila morphogens bicoid and hunchback. EMBO J. 1991
946 Aug;10(8):2267–2278.

947 6. Clark E, Peel AD, Akam M. Arthropod segmentation. Development. 2019 Sep 25;146(18).

948 7. Lynch JA, El-Sherif E, Brown SJ. Comparisons of the embryonic development of Drosophila,
949 Nasonia, and Tribolium. Wiley Interdiscip Rev Dev Biol. 2012 Feb;1(1):16–39.

950 8. Jaeger J. The gap gene network. Cell Mol Life Sci. 2011 Jan;68(2):243–274.

951 9. Diaz-Cuadros M, Pourquié O, El-Sherif E. Patterning with clocks and genetic cascades:
952 Segmentation and regionalization of vertebrate versus insect body plans. PLoS Genet. 2021 Oct
953 14;17(10):e1009812.

954 10. Di Talia S, Vergassola M. Waves in embryonic development. Annu Rev Biophys. 2022 May
955 9;51:327–353.

956 11. Palmeirim I, Henrique D, Ish-Horowicz D, Pourquié O. Avian hairy gene expression identifies a
957 molecular clock linked to vertebrate segmentation and somitogenesis. Cell. 1997 Nov
958 28;91(5):639–648.

959 12. Oates AC, Morelli LG, Ares S. Patterning embryos with oscillations: structure, function and
960 dynamics of the vertebrate segmentation clock. Development. 2012 Feb;139(4):625–639.

961 13. Lauschke VM, Tsiairis CD, François P, Aulehla A. Scaling of embryonic patterning based on phase-
962 gradient encoding. Nature. 2013 Jan 3;493(7430):101–105.

963 14. Aulehla A, Wiegraebe W, Baubet V, Wahl MB, Deng C, Taketo M, et al. A beta-catenin gradient
964 links the clock and wavefront systems in mouse embryo segmentation. Nat Cell Biol. 2008 Feb
965 1;10(2):186–193.

966 15. Soroldoni D, Jörg DJ, Morelli LG, Richmond DL, Schindelin J, Jülicher F, et al. Genetic oscillations.
967 A Doppler effect in embryonic pattern formation. Science. 2014 Jul 11;345(6193):222–225.

968 16. Sonnen KF, Janda CY. Signalling dynamics in embryonic development. Biochem J. 2021 Dec
969 10;478(23):4045–4070.

970 17. Forlani S, Lawson KA, Deschamps J. Acquisition of Hox codes during gastrulation and axial
971 elongation in the mouse embryo. Development. 2003 Aug 1;130(16):3807–3819.

972 18. Gaunt SJ, Strachan L. Forward spreading in the establishment of a vertebrate Hox expression
973 boundary: the expression domain separates into anterior and posterior zones, and the spread
974 occurs across implanted glass barriers. Dev Dyn. 1994 Mar;199(3):229–240.

975 19. Deschamps J, Duboule D. Embryonic timing, axial stem cells, chromatin dynamics, and the Hox
976 clock. Genes Dev. 2017 Jul 15;31(14):1406–1416.

977 20. Durston A, Wacker S, Bardine N, Jansen H. Time space translation: a hox mechanism for
978 vertebrate a-p patterning. Curr Genomics. 2012 Jun;13(4):300–307.

979 21. Durston AJ, Jansen HJ, Wacker SA. Review: Time-space translation regulates trunk axial
980 patterning in the early vertebrate embryo. Genomics. 2010 May;95(5):250–255.

981 22. Dessaud E, Yang LL, Hill K, Cox B, Ulloa F, Ribeiro A, et al. Interpretation of the sonic hedgehog
982 morphogen gradient by a temporal adaptation mechanism. Nature. 2007 Nov 29;450(7170):717–
983 720.

984 23. Balaskas N, Ribeiro A, Panovska J, Dessaud E, Sasai N, Page KM, et al. Gene regulatory logic for
985 reading the Sonic Hedgehog signaling gradient in the vertebrate neural tube. Cell. 2012 Jan
986 20;148(1-2):273–284.

987 24. Harfe BD, Scherz PJ, Nissim S, Tian H, McMahon AP, Tabin CJ. Evidence for an expansion-based
988 temporal Shh gradient in specifying vertebrate digit identities. Cell. 2004 Aug 20;118(4):517–528.

989 25. Saiz-Lopez P, Chinnaiya K, Campa VM, Delgado I, Ros MA, Towers M. An intrinsic timer specifies
990 distal structures of the vertebrate limb. Nat Commun. 2015 Sep 18;6:8108.

991 26. Roensch K, Tazaki A, Chara O, Tanaka EM. Progressive specification rather than intercalation of
992 segments during limb regeneration. Science. 2013 Dec 13;342(6164):1375–1379.

993 27. Towers M, Tickle C. Growing models of vertebrate limb development. Development. 2009
994 Jan;136(2):179–190.

995 28. El-Sherif E, Averof M, Brown SJ. A segmentation clock operating in blastoderm and germband
996 stages of Tribolium development. Development. 2012 Dec 1;139(23):4341–4346.

997 29. Sarrazin AF, Peel AD, Averof M. A segmentation clock with two-segment periodicity in insects.
998 Science. 2012 Apr 20;336(6079):338–341.

999 30. El-Sherif E, Zhu X, Fu J, Brown SJ. Caudal regulates the spatiotemporal dynamics of pair-rule
1000 waves in Tribolium. PLoS Genet. 2014 Oct 16;10(10):e1004677.

1001 31. Zhu X, Rudolf H, Healey L, François P, Brown SJ, Klingler M, et al. Speed regulation of genetic
1002 cascades allows for evolvability in the body plan specification of insects. Proc Natl Acad Sci USA.
1003 2017 Sep 25;114(41).

1004 32. Boos A, Distler J, Rudolf H, Klingler M, El-Sherif E. A re-inducible gap gene cascade patterns the
1005 anterior-posterior axis of insects in a threshold-free fashion. Elife. 2018 Dec 20;7.

1006 33. Brena C, Akam M. An analysis of segmentation dynamics throughout embryogenesis in the
1007 centipede Strigamia maritima. BMC Biol. 2013 Nov 29;11:112.

1008 34. Pueyo JI, Lanfear R, Couso JP. Ancestral Notch-mediated segmentation revealed in the cockroach
1009 Periplaneta americana. Proc Natl Acad Sci USA. 2008 Oct 28;105(43):16614–16619.

1010 35. Stollewerk A, Schoppmeier M, Damen WGM. Involvement of Notch and Delta genes in spider
1011 segmentation. Nature. 2003 Jun 19;423(6942):863–865.

1012 36. Rosenberg MI, Brent AE, Payre F, Desplan C. Dual mode of embryonic development is highlighted
1013 by expression and function of Nasonia pair-rule genes. Elife. 2014 Mar 5;3(3):e01440.

1014 37. Kanayama M, Akiyama-Oda Y, Nishimura O, Tarui H, Agata K, Oda H. Travelling and splitting of a
1015 wave of hedgehog expression involved in spider-head segmentation. Nat Commun. 2011 Oct
1016 11;2:500.

1017 38. Chipman AD, Akam M. The segmentation cascade in the centipede Strigamia maritima:
1018 involvement of the Notch pathway and pair-rule gene homologues. Dev Biol. 2008 Jul
1019 1;319(1):160–169.

1020 39. Pechmann M, McGregor AP, Schwager EE, Feitosa NM, Damen WGM. Dynamic gene expression
1021 is required for anterior regionalization in a spider. Proc Natl Acad Sci USA. 2009 Feb
1022 3;106(5):1468–1472.

1023 40. Jaeger J, Surkova S, Blagov M, Janssens H, Kosman D, Kozlov KN, et al. Dynamic control of
1024 positional information in the early Drosophila embryo. Nature. 2004 Jul 15;430(6997):368–371.

1025 41. El-Sherif E, Levine M. Shadow enhancers mediate dynamic shifts of gap gene expression in the
1026 drosophila embryo. Curr Biol. 2016 May 9;26(9):1164–1169.

1027 42. Lim B, Fukaya T, Heist T, Levine M. Temporal dynamics of pair-rule stripes in living Drosophila
1028 embryos. Proc Natl Acad Sci USA. 2018 Aug 14;115(33):8376–8381.

1029 43. Berrocal A, Lammers NC, Garcia HG, Eisen MB. Kinetic sculpting of the seven stripes of the
1030 Drosophila even-skipped gene. Elife. 2020 Dec 10;9.

1031 44. Keränen SVE, Fowlkes CC, Luengo Hendriks CL, Sudar D, Knowles DW, Malik J, et al. Three-
1032 dimensional morphology and gene expression in the Drosophila blastoderm at cellular resolution
1033 II: dynamics. Genome Biol. 2006;7(12):R124.

1034 45. Rudolf H, Zellner C, El-Sherif E. Speeding up anterior-posterior patterning of insects by
1035 differential initialization of the gap gene cascade. Dev Biol. 2020 Apr 1;460(1):20–31.

1036 46. Verd B, Clark E, Wotton KR, Janssens H, Jiménez-Guri E, Crombach A, et al. A damped oscillator
1037 imposes temporal order on posterior gap gene expression in Drosophila. PLoS Biol. 2018 Feb
1038 16;16(2):e2003174.

1039 47. Clark E, Peel AD. Evidence for the temporal regulation of insect segmentation by a conserved
1040 sequence of transcription factors. Development. 2018 May 3;

1041 48. Clark E. Dynamic patterning by the Drosophila pair-rule network reconciles long-germ and short-
1042 germ segmentation. PLoS Biol. 2017 Sep 27;15(9):e2002439.

1043 49. Kuhlmann L, El-Sherif E. Speed regulation and gradual enhancer switching models as flexible and
1044 evolvable patterning mechanisms. BioRxiv. 2018 Feb 7;

1045 50. Falk HJ, Tomita T, Mönke G, McDole K, Aulehla A. Imaging the onset of oscillatory signaling
1046 dynamics during mouse embryo gastrulation. Development. 2022 Jul 1;149(13).

1047 51. Diaz-Cuadros M, Wagner DE, Budjan C, Hubaud A, Tarazona OA, Donelly S, et al. In vitro
1048 characterization of the human segmentation clock. Nature. 2020 Apr;580(7801):113–118.

1049 52. Shih NP, François P, Delaune EA, Amacher SL. Dynamics of the slowing segmentation clock reveal
1050 alternating two-segment periodicity. Development. 2015 May 15;142(10):1785–1793.

1051 53. Hoermann A, Cicin-Sain D, Jaeger J. A quantitative validated model reveals two phases of
1052 transcriptional regulation for the gap gene giant in Drosophila. Dev Biol. 2016 Mar
1053 15;411(2):325–338.

1054 54. Oginuma M, Takahashi Y, Kitajima S, Kiso M, Kanno J, Kimura A, et al. The oscillation of Notch
1055 activation, but not its boundary, is required for somite border formation and rostral-caudal
1056 patterning within a somite. Development. 2010 May;137(9):1515–1522.

1057 55. Shifley ET, Vanhorn KM, Perez-Balaguer A, Franklin JD, Weinstein M, Cole SE. Oscillatory lunatic
1058 fringe activity is crucial for segmentation of the anterior but not posterior skeleton.
1059 Development. 2008 Mar;135(5):899–908.

1060 56. Stauber M, Sachidanandan C, Morgenstern C, Ish-Horowicz D. Differential axial requirements for
1061 lunatic fringe and Hes7 transcription during mouse somitogenesis. PLoS One. 2009 Nov
1062 24;4(11):e7996.

1063 57. Schroeder MD, Greer C, Gaul U. How to make stripes: deciphering the transition from non-
1064 periodic to periodic patterns in Drosophila segmentation. Development. 2011 Jul;138(14):3067–
1065 3078.

1066 58. Schroeder MD, Pearce M, Fak J, Fan H, Unnerstall U, Emberly E, et al. Transcriptional control in
1067 the segmentation gene network of Drosophila. PLoS Biol. 2004 Sep;2(9):E271.

1068 59. Bucher G, Scholten J, Klingler M. Parental rnai in tribolium (coleoptera). Curr Biol. 2002 Feb
1069 5;12(3):R85–6.

1070 60. Miller SC, Miyata K, Brown SJ, Tomoyasu Y. Dissecting systemic RNA interference in the red flour
1071 beetle Tribolium castaneum: parameters affecting the efficiency of RNAi. PLoS One. 2012 Oct
1072 25;7(10):e47431.

1073 61. Tomoyasu Y, Miller SC, Tomita S, Schoppmeier M, Grossmann D, Bucher G. Exploring systemic
1074 RNA interference in insects: a genome-wide survey for RNAi genes in Tribolium. Genome Biol.
1075 2008 Jan 17;9(1):R10.

1076 62. Dönitz J, Schmitt-Engel C, Grossmann D, Gerischer L, Tech M, Schoppmeier M, et al. iBeetle-Base:
1077 a database for RNAi phenotypes in the red flour beetle Tribolium castaneum. Nucleic Acids Res.
1078 2015 Jan;43(Database issue):D720–5.

1079 63. Choe CP, Brown SJ. Genetic regulation of engrailed and wingless in Tribolium segmentation and
1080 the evolution of pair-rule segmentation. Dev Biol. 2009 Jan 15;325(2):482–491.

1081 64. Bolognesi R, Beermann A, Farzana L, Wittkopp N, Lutz R, Balavoine G, et al. Tribolium Wnts:
1082 evidence for a larger repertoire in insects with overlapping expression patterns that suggest
1083 multiple redundant functions in embryogenesis. Dev Genes Evol. 2008 Apr 8;218(3-4):193–202.

1084 65. Choe CP, Miller SC, Brown SJ. A pair-rule gene circuit defines segments sequentially in the short-
1085 germ insect Tribolium castaneum. Proc Natl Acad Sci USA. 2006 Apr 25;103(17):6560–6564.

1086 66. Kotkamp K, Klingler M, Schoppmeier M. Apparent role of Tribolium orthodenticle in
1087 anteroposterior blastoderm patterning largely reflects novel functions in dorsoventral axis
1088 formation and cell survival. Development. 2010 Jun;137(11):1853–1862.

1089 67. Schoppmeier M, Fischer S, Schmitt-Engel C, Löhr U, Klingler M. An ancient anterior patterning
1090 system promotes caudal repression and head formation in ecdysozoa. Curr Biol. 2009 Nov
1091 17;19(21):1811–1815.

1092 68. Cerny AC, Bucher G, Schröder R, Klingler M. Breakdown of abdominal patterning in the Tribolium
1093 Kruppel mutant jaws. Development. 2005 Dec;132(24):5353–5363.

1094 69. Bucher G, Klingler M. Divergent segmentation mechanism in the short germ insect Tribolium
1095 revealed by giant expression and function. Development. 2004 Apr;131(8):1729–1740.

1096 70. Schmitt-Engel C, Cerny AC, Schoppmeier M. A dual role for nanos and pumilio in anterior and
1097 posterior blastodermal patterning of the short-germ beetle Tribolium castaneum. Dev Biol. 2012
1098 Apr 15;364(2):224–235.

1099 71. Marques-Souza H, Aranda M, Tautz D. Delimiting the conserved features of hunchback function
1100 for the trunk organization of insects. Development. 2008 Mar;135(5):881–888.

1101 72. Savard J, Marques-Souza H, Aranda M, Tautz D. A segmentation gene in tribolium produces a
1102 polycistronic mRNA that codes for multiple conserved peptides. Cell. 2006 Aug 11;126(3):559–
1103 569.

1104 73. Marques-Souza H. Evolution of the gene regulatory network controlling trunk segmentation in
1105 insects [Doctoral dissertation]. University of Cologne; 2007.

1106 74. Jeon H, Gim S, Na H, Choe CP. A pair-rule function of odd-skipped in germband stages of
1107 Tribolium development. Dev Biol. 2020 Jul 17;

1108 75. Klingler M, Bucher G. The red flour beetle T. castaneum: elaborate genetic toolkit and unbiased
1109 large scale RNAi screening to study insect biology and evolution. Evodevo. 2022 Dec;13(1):14.

1110 76. Pavlopoulos A, Berghammer AJ, Averof M, Klingler M. Efficient transformation of the beetle
1111 Tribolium castaneum using the Minos transposable element: quantitative and qualitative
1112 analysis of genomic integration events. Genetics. 2004 Jun;167(2):737–746.

1113 77. Strobl F, Anderl A, Stelzer EH. A universal vector concept for a direct genotyping of transgenic
1114 organisms and a systematic creation of homozygous lines. Elife. 2018 Mar 15;7.

1115 78. Trauner J, Schinko J, Lorenzen MD, Shippy TD, Wimmer EA, Beeman RW, et al. Large-scale
1116 insertional mutagenesis of a coleopteran stored grain pest, the red flour beetle Tribolium
1117 castaneum, identifies embryonic lethal mutations and enhancer traps. BMC Biol. 2009 Nov
1118 5;7:73.

1119 79. Gilles AF, Schinko JB, Averof M. Efficient CRISPR-mediated gene targeting and transgene
1120 replacement in the beetle Tribolium castaneum. Development. 2015 Aug 15;142(16):2832–2839.

1121 80. Gilles AF, Schinko JB, Schacht MI, Enjolras C, Averof M. Clonal analysis by tunable CRISPR-
1122 mediated excision. Development. 2019 Jan 4;146(1).

1123 81. Strobl F, Stelzer EH. Long-term fluorescence live imaging of Tribolium castaneum embryos:
1124 principles, resources, scientific challenges and the comparative approach. Curr Opin Insect Sci.
1125 2016 Aug 28;18:17–26.

1126 82. Strobl F, Stelzer EHK. Non-invasive long-term fluorescence live imaging of Tribolium castaneum
1127 embryos. Development. 2014 Jun;141(11):2331–2338.

1128 83. Strobl F, Schmitz A, Stelzer EHK. Live imaging of Tribolium castaneum embryonic development
1129 using light-sheet-based fluorescence microscopy. Nat Protoc. 2015 Oct;10(10):1486–1507.

1130 84. Macaya CC, Saavedra PE, Cepeda RE, Nuñez VA, Sarrazin AF. A Tribolium castaneum whole-
1131 embryo culture protocol for studying the molecular mechanisms and morphogenetic movements
1132 involved in insect development. Dev Genes Evol. 2016 Jan 6;226(1):53–61.

1133 85. Buenrostro JD, Giresi PG, Zaba LC, Chang HY, Greenleaf WJ. Transposition of native chromatin for
1134 fast and sensitive epigenomic profiling of open chromatin, DNA-binding proteins and
1135 nucleosome position. Nat Methods. 2013 Dec;10(12):1213–1218.

1136 86. Thurman RE, Rynes E, Humbert R, Vierstra J, Maurano MT, Haugen E, et al. The accessible
1137 chromatin landscape of the human genome. Nature. 2012 Sep 6;489(7414):75–82.

1138 87. Kok K, Arnosti DN. Dynamic reprogramming of chromatin: paradigmatic palimpsests and HES
1139 factors. Front Genet. 2015 Feb 10;6:29.

1140 88. Xi H, Shulha HP, Lin JM, Vales TR, Fu Y, Bodine DM, et al. Identification and characterization of
1141 cell type-specific and ubiquitous chromatin regulatory structures in the human genome. PLoS
1142 Genet. 2007 Aug;3(8):e136.

1143 89. Li LM, Arnosti DN. Long- and short-range transcriptional repressors induce distinct chromatin
1144 states on repressed genes. Curr Biol. 2011 Mar 8;21(5):406–412.

1145 90. Reddington JP, Garfield DA, Sigalova OM, Karabacak Calviello A, Marco-Ferreres R, Girardot C, et
1146 al. Lineage-Resolved Enhancer and Promoter Usage during a Time Course of Embryogenesis. Dev
1147 Cell. 2020 Dec 7;55(5):648–664.e9.

1148 91. Bozek M, Cortini R, Storti AE, Unnerstall U, Gaul U, Gompel N. ATAC-seq reveals regional
1149 differences in enhancer accessibility during the establishment of spatial coordinates in the
1150 Drosophila blastoderm. Genome Res. 2019 May;29(5):771–783.

1151 92. McKay DJ, Lieb JD. A common set of DNA regulatory elements shapes Drosophila appendages.
1152 Dev Cell. 2013 Nov 11;27(3):306–318.

1153 93. Li X, Zhao X, Fang Y, Jiang X, Duong T, Fan C, et al. Generation of destabilized green fluorescent
1154 protein as a transcription reporter. J Biol Chem. 1998 Dec 25;273(52):34970–34975.

1155 94. He L, Binari R, Huang J, Falo-Sanjuan J, Perrimon N. In vivo study of gene expression with an
1156 enhanced dual-color fluorescent transcriptional timer. Elife. 2019 May 29;8.

1157 95. Pichon X, Lagha M, Mueller F, Bertrand E. A growing toolbox to image gene expression in single
1158 cells: sensitive approaches for demanding challenges. Mol Cell. 2018 Aug 2;71(3):468–480.

1159 96. Johansson HE, Liljas L, Uhlenbeck OC. RNA recognition by the MS2 phage coat protein. Seminars
1160 in virology. 1997;8(3):176–185.

1161 97. Garcia HG, Tikhonov M, Lin A, Gregor T. Quantitative imaging of transcription in living Drosophila
1162 embryos links polymerase activity to patterning. Curr Biol. 2013 Nov 4;23(21):2140–2145.

1163 98. Lucas T, Ferraro T, Roelens B, De Las Heras Chanes J, Walczak AM, Coppey M, et al. Live imaging
1164 of bicoid-dependent transcription in Drosophila embryos. Curr Biol. 2013 Nov 4;23(21):2135–
1165 2139.

1166 99. Bothma JP, Garcia HG, Esposito E, Schlissel G, Gregor T, Levine M. Dynamic regulation of eve
1167 stripe 2 expression reveals transcriptional bursts in living Drosophila embryos. Proc Natl Acad Sci
1168 USA. 2014 Jul 22;111(29):10598–10603.

1169 100. Simon JM, Giresi PG, Davis IJ, Lieb JD. Using formaldehyde-assisted isolation of regulatory
1170 elements (FAIRE) to isolate active regulatory DNA. Nat Protoc. 2012 Jan 19;7(2):256–267.

1171 101. Lai Y-T, Deem KD, Borràs-Castells F, Sambrani N, Rudolf H, Suryamohan K, et al. Enhancer
1172 identification and activity evaluation in the red flour beetle, Tribolium castaneum. Development.
1173 2018 Apr 5;145(7).

1174 102. Perry MW, Boettiger AN, Levine M. Multiple enhancers ensure precision of gap gene-expression
1175 patterns in the Drosophila embryo. Proc Natl Acad Sci USA. 2011 Aug 16;108(33):13570–13575.

1176 103. Choi HMT, Schwarzkopf M, Fornace ME, Acharya A, Artavanis G, Stegmaier J, et al. Third-
1177 generation in situ hybridization chain reaction: multiplexed, quantitative, sensitive, versatile,
1178 robust. Development. 2018 Jun 26;145(12).

1179 104. Cande J, Goltsev Y, Levine MS. Conservation of enhancer location in divergent insects. Proc Natl
1180 Acad Sci USA. 2009 Aug 25;106(34):14414–14419.

1181 105. Schönauer A, Paese CLB, Hilbrant M, Leite DJ, Schwager EE, Feitosa NM, et al. The Wnt and
1182 Delta-Notch signalling pathways interact to direct pair-rule gene expression via caudal during
1183 segment addition in the spider Parasteatoda tepidariorum. Development. 2016 Jul
1184 1;143(13):2455–2463.

1185 106. Bolognesi R, Farzana L, Fischer TD, Brown SJ. Multiple Wnt genes are required for segmentation
1186 in the short-germ embryo of Tribolium castaneum. Curr Biol. 2008 Oct 28;18(20):1624–1629.

1187 107. Copf T, Schröder R, Averof M. Ancestral role of caudal genes in axis elongation and
1188 segmentation. Proc Natl Acad Sci USA. 2004 Dec 21;101(51):17711–17715.

1189 108. McGregor AP, Pechmann M, Schwager EE, Feitosa NM, Kruck S, Aranda M, et al. Wnt8 is
1190 required for growth-zone establishment and development of opisthosomal segments in a spider.
1191 Curr Biol. 2008 Oct 28;18(20):1619–1623.

1192 109. Bailles A, Gehrels EW, Lecuit T. Mechanochemical principles of spatial and temporal patterns in
1193 cells and tissues. Annu Rev Cell Dev Biol. 2022 May 13;

1194 110. Jouve C, Iimura T, Pourquie O. Onset of the segmentation clock in the chick embryo: evidence for
1195 oscillations in the somite precursors in the primitive streak. Development. 2002
1196 Mar;129(5):1107–1117.

1197 111. Jutras-Dubé L, El-Sherif E, François P. Geometric models for robust encoding of dynamical
1198 information into embryonic patterns. Elife. 2020 Aug 10;9.

1199 112. Vroomans RMA, Hogeweg P, Ten Tusscher KHWJ. Around the clock: gradient shape and noise
1200 impact the evolution of oscillatory segmentation dynamics. Evodevo. 2018 Dec 10;9:24.

1201 113. Winfree AT. The Geometry of Biological Time (Interdisciplinary Applied Mathematics). 2nd ed.
1202 2001. Softcover reprint of the original 2nd ed. 2001. Springer; 2010.

1203 114. Rayon T, Stamataki D, Perez-Carrasco R, Garcia-Perez L, Barrington C, Melchionda M, et al.
1204 Species-specific pace of development is associated with differences in protein stability. Science.
1205 2020 Sep 18;369(6510).

1206 115. Uyehara CM, Nystrom SL, Niederhuber MJ, Leatham-Jensen M, Ma Y, Buttitta LA, et al.
1207 Hormone-dependent control of developmental timing through regulation of chromatin
1208 accessibility. Genes Dev. 2017 May 1;31(9):862–875.

1209 116. Pease NA, Nguyen PHB, Woodworth MA, Ng KKH, Irwin B, Vaughan JC, et al. Tunable, division-
1210 independent control of gene activation timing by a polycomb switch. Cell Rep. 2021 Mar
1211 23;34(12):108888.

1212 117. Nguyen P, Pease NA, Kueh HY. Scalable control of developmental timetables by epigenetic
1213 switching networks. J R Soc Interface. 2021 Jul 21;18(180):20210109.

1214 118. Benito-Kwiecinski S, Giandomenico SL, Sutcliffe M, Riis ES, Freire-Pritchett P, Kelava I, et al. An
1215 early cell shape transition drives evolutionary expansion of the human forebrain. Cell. 2021 Apr
1216 15;184(8):2084–2102.e19.

1217 119. Bielen H, Pal S, Tole S, Houart C. Temporal variations in early developmental decisions: an engine
1218 of forebrain evolution. Curr Opin Neurobiol. 2017 Feb;42:152–159.

1219 120. Preger-Ben Noon E, Sabarís G, Ortiz DM, Sager J, Liebowitz A, Stern DL, et al. Comprehensive
1220 Analysis of a cis-Regulatory Region Reveals Pleiotropy in Enhancer Function. Cell Rep. 2018 Mar
1221 13;22(11):3021–3031.

1222 121. Sabarís G, Laiker I, Preger-Ben Noon E, Frankel N. Actors with Multiple Roles: Pleiotropic
1223 Enhancers and the Paradigm of Enhancer Modularity. Trends Genet. 2019 Jun;35(6):423–433.

1224 122. Lewis JJ, Geltman RC, Pollak PC, Rondem KE, Van Belleghem SM, Hubisz MJ, et al. Parallel
1225 evolution of ancient, pleiotropic enhancers underlies butterfly wing pattern mimicry. Proc Natl
1226 Acad Sci USA. 2019 Nov 26;116(48):24174–24183.

1227 123. Murugesan SN, Connahs H, Matsuoka Y, Das Gupta M, Tiong GJL, Huq M, et al. Butterfly
1228 eyespots evolved via cooption of an ancestral gene-regulatory network that also patterns
1229 antennae, legs, and wings. Proc Natl Acad Sci USA. 2022 Feb 22;119(8).

1230 124. Erceg J, Pakozdi T, Marco-Ferreres R, Ghavi-Helm Y, Girardot C, Bracken AP, et al. Dual
1231 functionality of cis-regulatory elements as developmental enhancers and Polycomb response
1232 elements. Genes Dev. 2017 Mar 15;31(6):590–602.

1233 125. Arnosti DN, Barolo S, Levine M, Small S. The eve stripe 2 enhancer employs multiple modes of
1234 transcriptional synergy. Development. 1996 Jan;122(1):205–214.

1235 126. Howard K, Ingham P, Rushlow C. Region-specific alleles of the Drosophila segmentation gene
1236 hairy. Genes Dev. 1988 Aug;2(8):1037–1046.

1237 127. Estella C, Voutev R, Mann RS. A dynamic network of morphogens and transcription factors
1238 patterns the fly leg. Curr Top Dev Biol. 2012;98:173–198.

1239 128. Clark E, Akam M. Odd-paired controls frequency doubling in Drosophila segmentation by altering
1240 the pair-rule gene regulatory network. Elife. 2016 Aug 15;5.

1241 129. Soluri IV, Zumerling LM, Payan Parra OA, Clark EG, Blythe SA. Zygotic pioneer factor activity of
1242 Odd-paired/Zic is necessary for late function of the Drosophila segmentation network. Elife.
1243 2020 Apr 29;9.

1244 130. Koromila T, Gao F, Iwasaki Y, He P, Pachter L, Gergen JP, et al. Odd-paired is a pioneer-like factor
1245 that coordinates with Zelda to control gene expression in embryos. Elife. 2020 Jul 23;9.

1246 131. Taylor SE, Dearden PK. The Nasonia pair-rule gene regulatory network retains its function over
1247 300 million years of evolution. Development. 2022 Mar 1;149(5).

1248 132. Ribeiro L, Tobias-Santos V, Santos D, Antunes F, Feltran G, de Souza Menezes J, et al. Evolution
1249 and multiple roles of the Pancrustacea specific transcription factor zelda in insects. PLoS Genet.
1250 2017 Jul 3;13(7):e1006868.

1251 133. Ng KK, Yui MA, Mehta A, Siu S, Irwin B, Pease S, et al. A stochastic epigenetic switch controls the
1252 dynamics of T-cell lineage commitment. Elife. 2018 Nov 20;7.

1253 134. Ay A, Holland J, Sperlea A, Devakanmalai GS, Knierer S, Sangervasi S, et al. Spatial gradients of
1254 protein-level time delays set the pace of the traveling segmentation clock waves. Development.
1255 2014 Nov;141(21):4158–4167.

1256 135. Okubo Y, Sugawara T, Abe-Koduka N, Kanno J, Kimura A, Saga Y. Lfng regulates the synchronized
1257 oscillation of the mouse segmentation clock via trans-repression of Notch signalling. Nat
1258 Commun. 2012;3:1141.

1259 136. Tsiairis CD, Aulehla A. Self-Organization of Embryonic Genetic Oscillators into Spatiotemporal
1260 Wave Patterns. Cell. 2016 Feb 11;164(4):656–667.

1261 137. Herrgen L, Ares S, Morelli LG, Schröter C, Jülicher F, Oates AC. Intercellular coupling regulates the
1262 period of the segmentation clock. Curr Biol. 2010 Jul 27;20(14):1244–1253.

1263 138. Yoshioka-Kobayashi K, Matsumiya M, Niino Y, Isomura A, Kori H, Miyawaki A, et al. Coupling
1264 delay controls synchronized oscillation in the segmentation clock. Nature. 2020
1265 Apr;580(7801):119–123.

1266 139. Morelli LG, Ares S, Herrgen L, Schröter C, Jülicher F, Oates AC. Delayed coupling theory of
1267 vertebrate segmentation. HFSP J. 2009;3(1):55–66.

1268 140. Liao B-K, Jörg DJ, Oates AC. Faster embryonic segmentation through elevated Delta-Notch
1269 signalling. Nat Commun. 2016 Jun 15;7:11861.

1270 141. Dönitz J, Gerischer L, Hahnke S, Pfeiffer S, Bucher G. Expanded and updated data and a query
1271 pipeline for iBeetle-Base. Nucleic Acids Res. 2018 Jan 4;46(D1):D831–D835.

1272 142. Pfeiffer BD, Jenett A, Hammonds AS, Ngo T-TB, Misra S, Murphy C, et al. Tools for neuroanatomy
1273 and neurogenetics in Drosophila. Proc Natl Acad Sci USA. 2008 Jul 15;105(28):9715–9720.

1274 143. Tribolium Genome Sequencing Consortium, Richards S, Gibbs RA, Weinstock GM, Brown SJ,
1275 Denell R, et al. The genome of the model beetle and pest Tribolium castaneum. Nature. 2008 Apr
1276 24;452(7190):949–955.

1277 144. Siebert KS, Lorenzen MD, Brown SJ, Park Y, Beeman RW. Tubulin superfamily genes in Tribolium
1278 castaneum and the use of a Tubulin promoter to drive transgene expression. Insect Biochem Mol
1279 Biol. 2008 Aug;38(8):749–755.

1280 145. Chook YM, Blobel G. Karyopherins and nuclear import. Curr Opin Struct Biol. 2001
1281 Dec;11(6):703–715.

1282 146. Field J, Nikawa J, Broek D, MacDonald B, Rodgers L, Wilson IA, et al. Purification of a RAS-
1283 responsive adenylyl cyclase complex from Saccharomyces cerevisiae by use of an epitope
1284 addition method. Mol Cell Biol. 1988 May;8(5):2159–2165.

1285 147. Bertrand E, Chartrand P, Schaefer M, Shenoy SM, Singer RH, Long RM. Localization of ASH1
1286 mRNA particles in living yeast. Mol Cell. 1998 Oct;2(4):437–445.

1287 148. Shaner NC, Steinbach PA, Tsien RY. A guide to choosing fluorescent proteins. Nat Methods. 2005
1288 Dec;2(12):905–909.

1289 149. Li X, Harrell RA, Handler AM, Beam T, Hennessy K, Fraser MJ. piggyBac internal sequences are
1290 necessary for efficient transformation of target genomes. Insect Mol Biol. 2005 Jan;14(1):17–30.

1291 150. Shaner NC, Lin MZ, McKeown MR, Steinbach PA, Hazelwood KL, Davidson MW, et al. Improving
1292 the photostability of bright monomeric orange and red fluorescent proteins. Nat Methods. 2008
1293 Jun;5(6):545–551.

1294 151. Shaner NC, Campbell RE, Steinbach PA, Giepmans BNG, Palmer AE, Tsien RY. Improved
1295 monomeric red, orange and yellow fluorescent proteins derived from Discosoma sp. red
1296 fluorescent protein. Nat Biotechnol. 2004 Dec;22(12):1567–1572.

1297 152. Berghammer AJ, Klingler M, Wimmer EA. A universal marker for transgenic insects. Nature. 1999
1298 Nov 25;402(6760):370–371.

1299 153. Handler AM, Harrell RA. Germline transformation of Drosophila melanogaster with the piggyBac
1300 transposon vector. Insect Mol Biol. 1999 Nov;8(4):449–457.

1301 154. Lorenzen MD, Berghammer AJ, Brown SJ, Denell RE, Klingler M, Beeman RW. piggyBac-mediated
1302 germline transformation in the beetle Tribolium castaneum. Insect Mol Biol. 2003
1303 Oct;12(5):433–440.

1304 155. Berghammer AJ, Weber M, Trauner J, Klingler M. Red flour beetle (Tribolium) germline
1305 transformation and insertional mutagenesis. Cold Spring Harb Protoc. 2009
1306 Aug;2009(8):pdb.prot5259.

1307 156. Lorenzen MD, Brown SJ, Denell RE, Beeman RW. Cloning and characterization of the Tribolium
1308 castaneum eye-color genes encoding tryptophan oxygenase and kynurenine 3-monooxygenase.
1309 Genetics. 2002 Jan;160(1):225–234.

1310 157. Handler AM. Use of the piggyBac transposon for germ-line transformation of insects. Insect
1311 Biochem Mol Biol. 2002 Oct;32(10):1211–1220.

1312 158. Schindelin J, Arganda-Carreras I, Frise E, Kaynig V, Longair M, Pietzsch T, et al. Fiji: an open-
1313 source platform for biological-image analysis. Nat Methods. 2012 Jun 28;9(7):676–682.

1314 159. Buenrostro JD, Wu B, Chang HY, Greenleaf WJ. ATAC-seq: a method for assaying chromatin
1315 accessibility genome-wide. Curr Protoc Mol Biol. 2015 Jan 5;109:21.29.1–21.29.9.

1316 160. Blythe SA, Wieschaus EF. Establishment and maintenance of heritable chromatin structure
1317 during early Drosophila embryogenesis. Elife. 2016 Nov 23;5.

1318 161. Martin M. Cutadapt removes adapter sequences from high-throughput sequencing reads.
1319 EMBnet j. 2011 May 2;17(1):10.

1320 162. Aligning sequence reads, clone sequences and assembly contigs with BWA-MEM – ScienceOpen
1321 [Internet]. [cited 2022 Oct 24]. Available from:
1322 https://www.scienceopen.com/document?vid=e623e045-f570-42c5-80c8-ef0aea06629c

1323 163. Danecek P, Bonfield JK, Liddle J, Marshall J, Ohan V, Pollard MO, et al. Twelve years of SAMtools
1324 and BCFtools. Gigascience. 2021 Feb 16;10(2).

1325 164. Amemiya HM, Kundaje A, Boyle AP. The ENCODE blacklist: identification of problematic regions
1326 of the genome. Sci Rep. 2019 Jun 27;9(1):9354.

1327 165. Pongor LS, Gross JM, Vera Alvarez R, Murai J, Jang S-M, Zhang H, et al. BAMscale: quantification
1328 of next-generation sequencing peaks and generation of scaled coverage tracks. Epigenetics
1329 Chromatin. 2020 Apr 22;13(1):21.

1330 166. Zhang Y, Liu T, Meyer CA, Eeckhoute J, Johnson DS, Bernstein BE, et al. Model-based analysis of
1331 ChIP-Seq (MACS). Genome Biol. 2008 Sep 17;9(9):R137.

1332 167. Heinz S, Benner C, Spann N, Bertolino E, Lin YC, Laslo P, et al. Simple combinations of lineage-
1333 determining transcription factors prime cis-regulatory elements required for macrophage and B
1334 cell identities. Mol Cell. 2010 May 28;38(4):576–589.

1335 168. Lopez-Delisle L, Rabbani L, Wolff J, Bhardwaj V, Backofen R, Grüning B, et al. pyGenomeTracks:
1336 reproducible plots for multivariate genomic datasets. Bioinformatics. 2021 Apr 20;37(3):422–
1337 423.

1338 169. Ramírez F, Bhardwaj V, Arrigoni L, Lam KC, Grüning BA, Villaveces J, et al. High-resolution TADs
1339 reveal DNA sequences underlying genome organization in flies. Nat Commun. 2018 Jan
1340 15;9(1):189.

1341 170. Robinson MD, McCarthy DJ, Smyth GK. edgeR: a Bioconductor package for differential
1342 expression analysis of digital gene expression data. Bioinformatics. 2010 Jan 1;26(1):139–140.

1343 171. Love MI, Huber W, Anders S. Moderated estimation of fold change and' ' dispersion for RNA-seq
1344 data with DESeq2. Genome Biol. 2014;15(12):550.

1345 172. Ross-Innes CS, Stark R, Teschendorff AE, Holmes KA, Ali HR, Dunning MJ, et al. Differential
1346 oestrogen receptor binding is associated with clinical outcome in breast cancer. Nature. 2012 Jan
1347 4;481(7381):389–393.

1348 173. Robinson MD, Oshlack A. A scaling normalization method for differential expression analysis of
1349 RNA-seq data. Genome Biol. 2010 Mar 2;11(3):R25.

1350 174. Grant CE, Bailey TL. XSTREME: Comprehensive motif analysis of biological sequence datasets.
1351 BioRxiv. 2021 Sep 3;

1352 175. Castro-Mondragon JA, Riudavets-Puig R, Rauluseviciute I, Lemma RB, Turchi L, Blanc-Mathieu R,
1353 et al. JASPAR 2022: the 9th release of the open-access database of transcription factor binding
1354 profiles. Nucleic Acids Res. 2022 Jan 7;50(D1):D165–D173.

1355

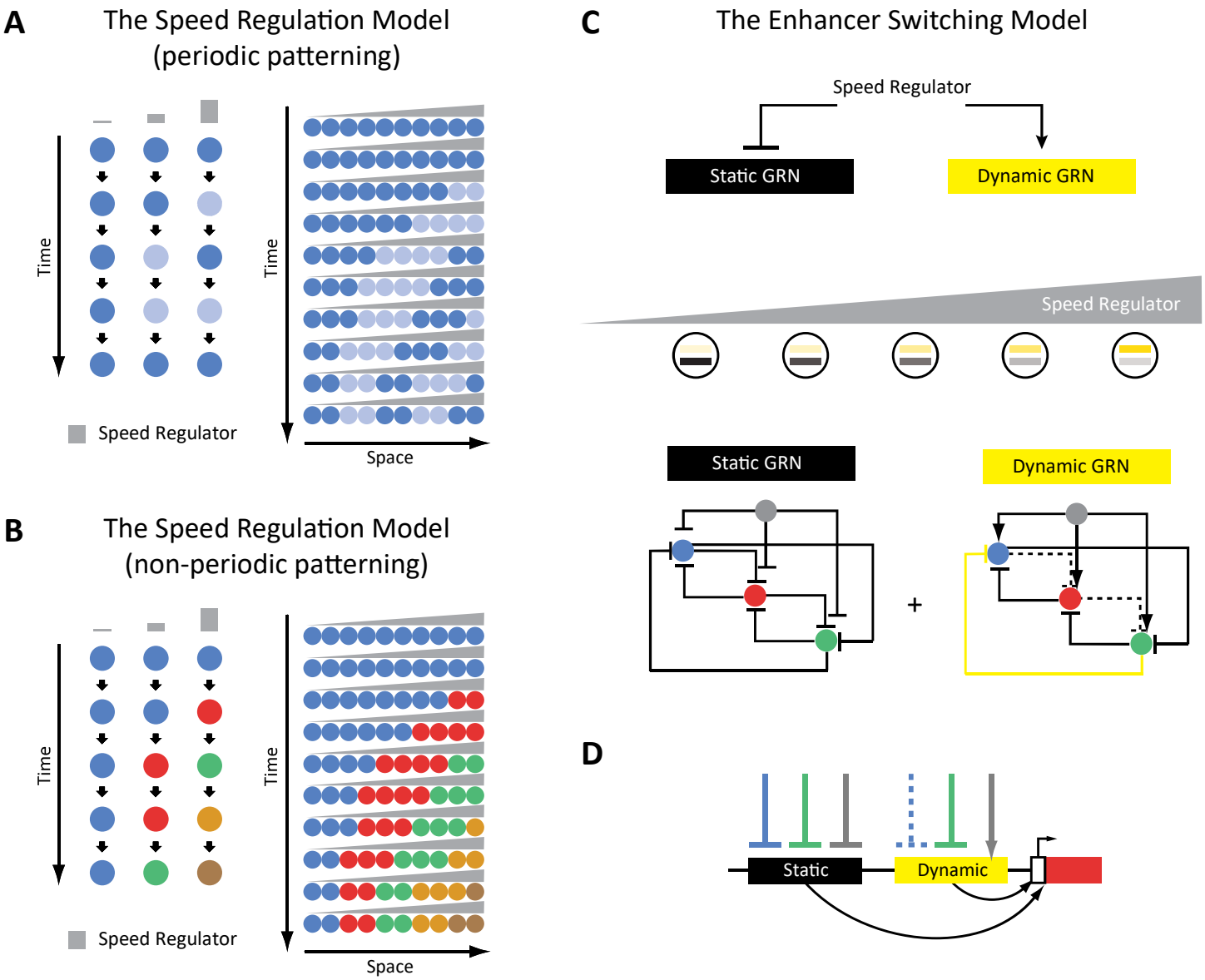


**Figure 1. The Enhancer Switching Model as a molecular realization of the Speed Regulation Model.**

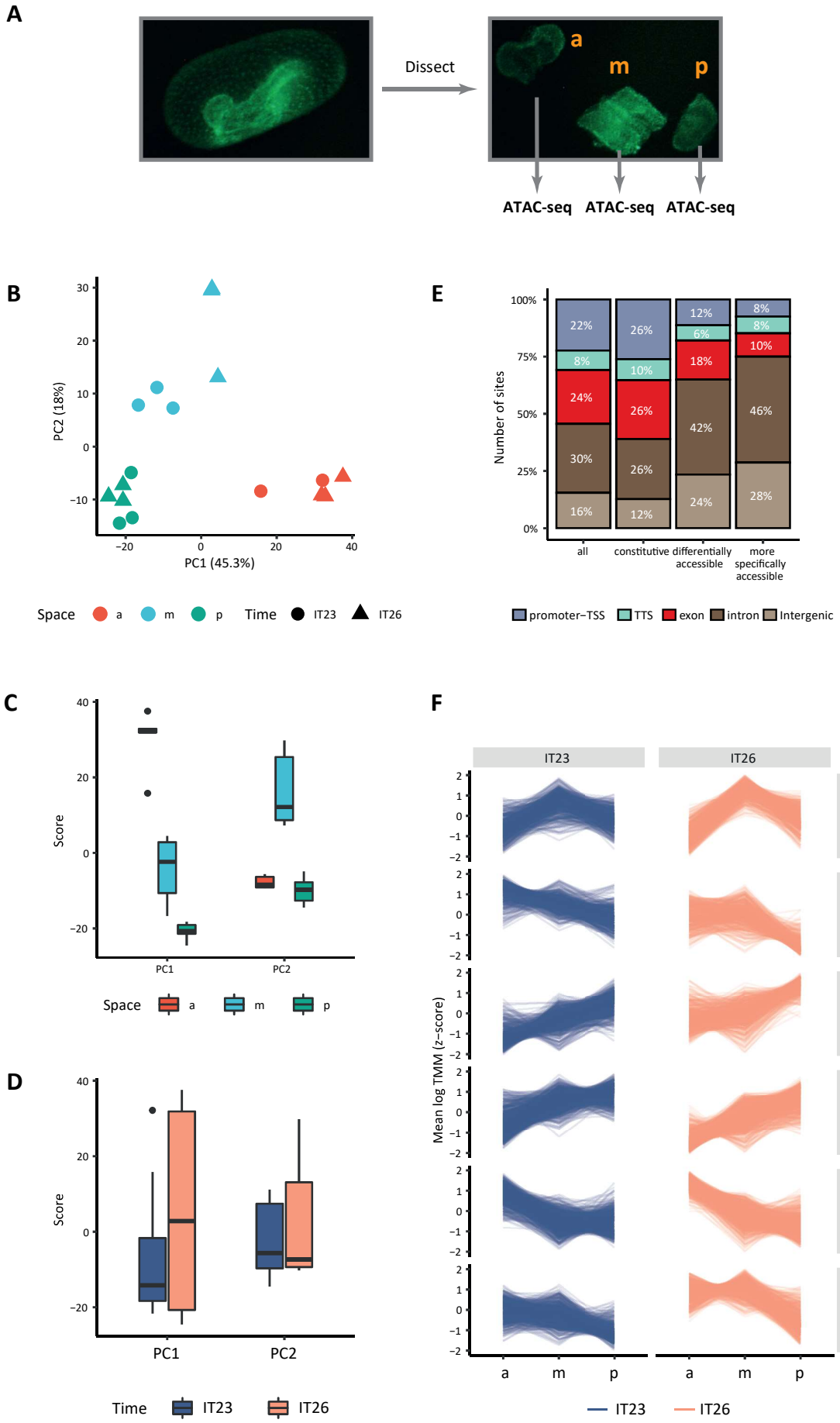


**Figure 2. Chromatin accessibility dynamics during AP patterning of the early *Tribolium* embryo.**

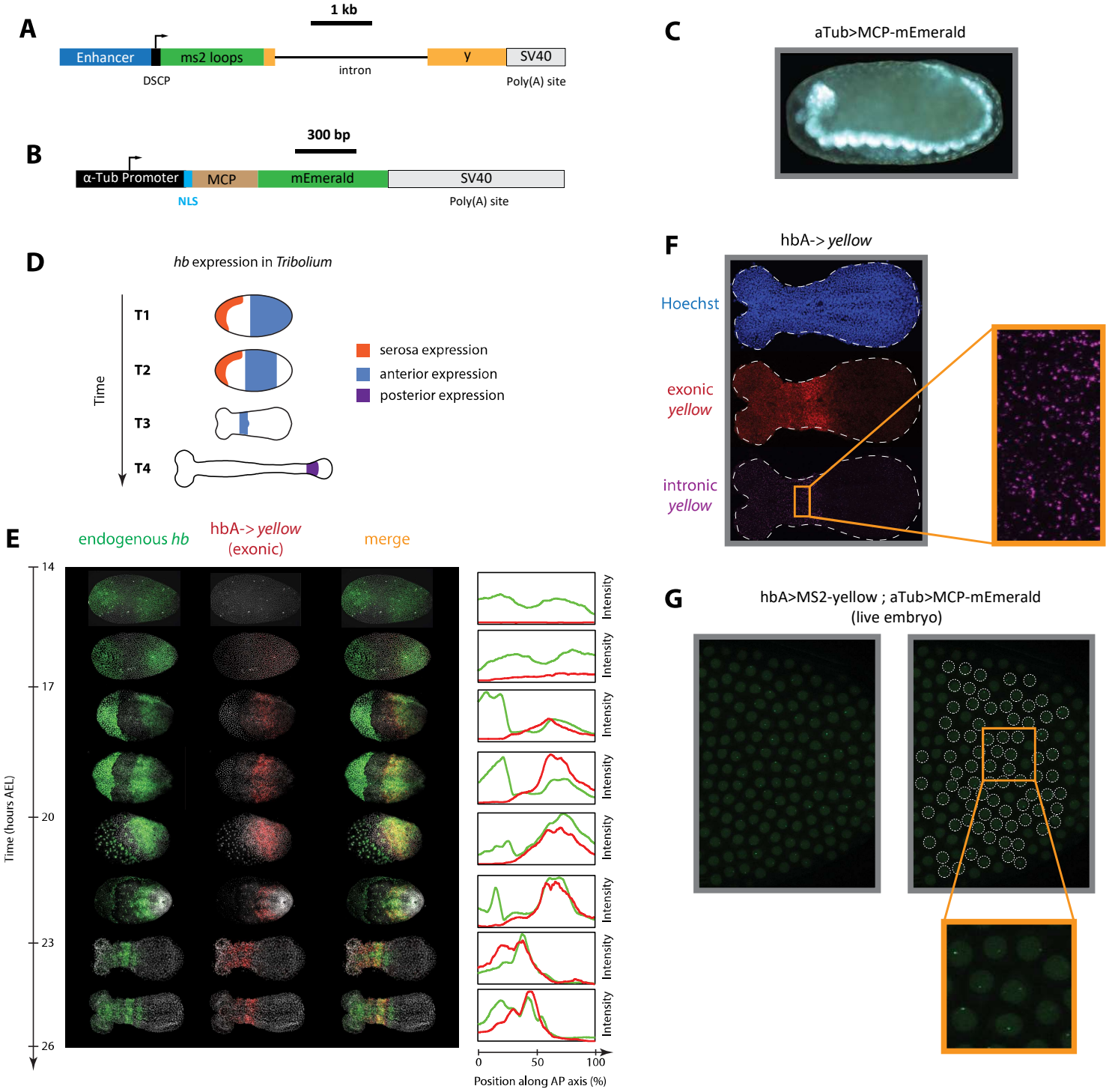


**Figure 3. An MS2-MCP enhancer reporter system to visualize enhancer activity in fixed and live *Tribolium* embryos tested using the *Tribolium hb* enhancer hbA.**

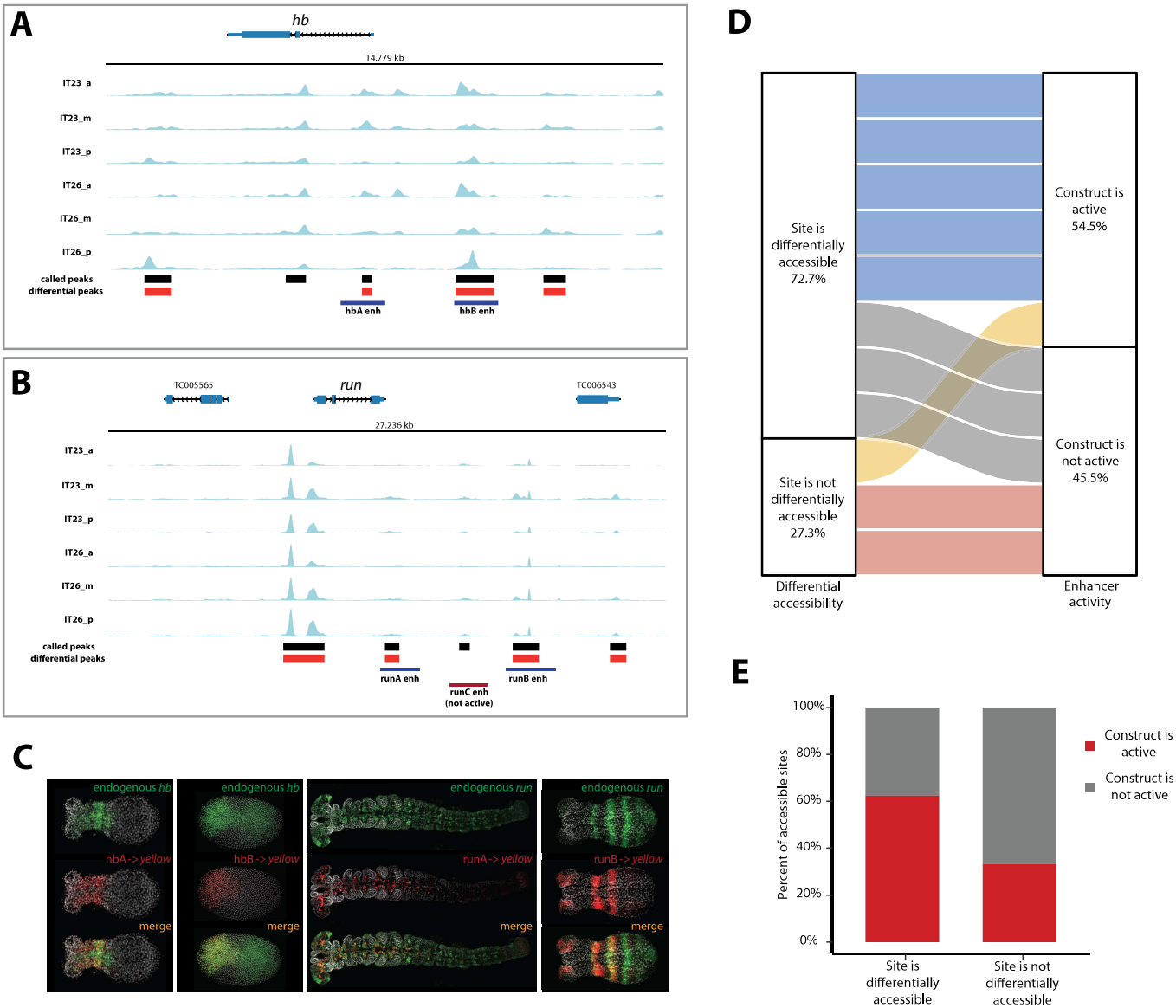


**Figure 4. Correlation of enhancer activity with differential accessibility.**

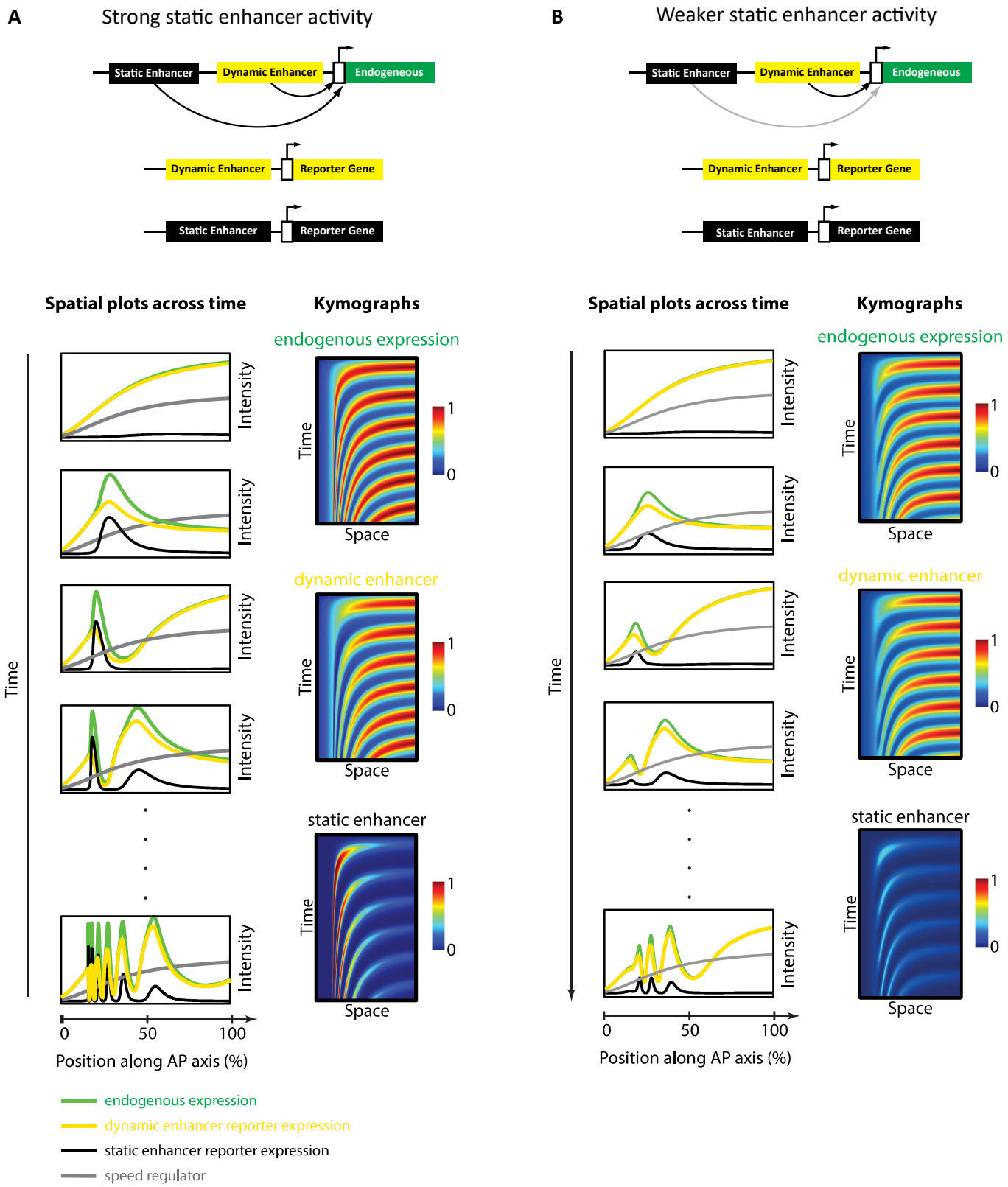


**Figure 5. Simulation of the Enhancer Switching model with different static enhancer strengths.**

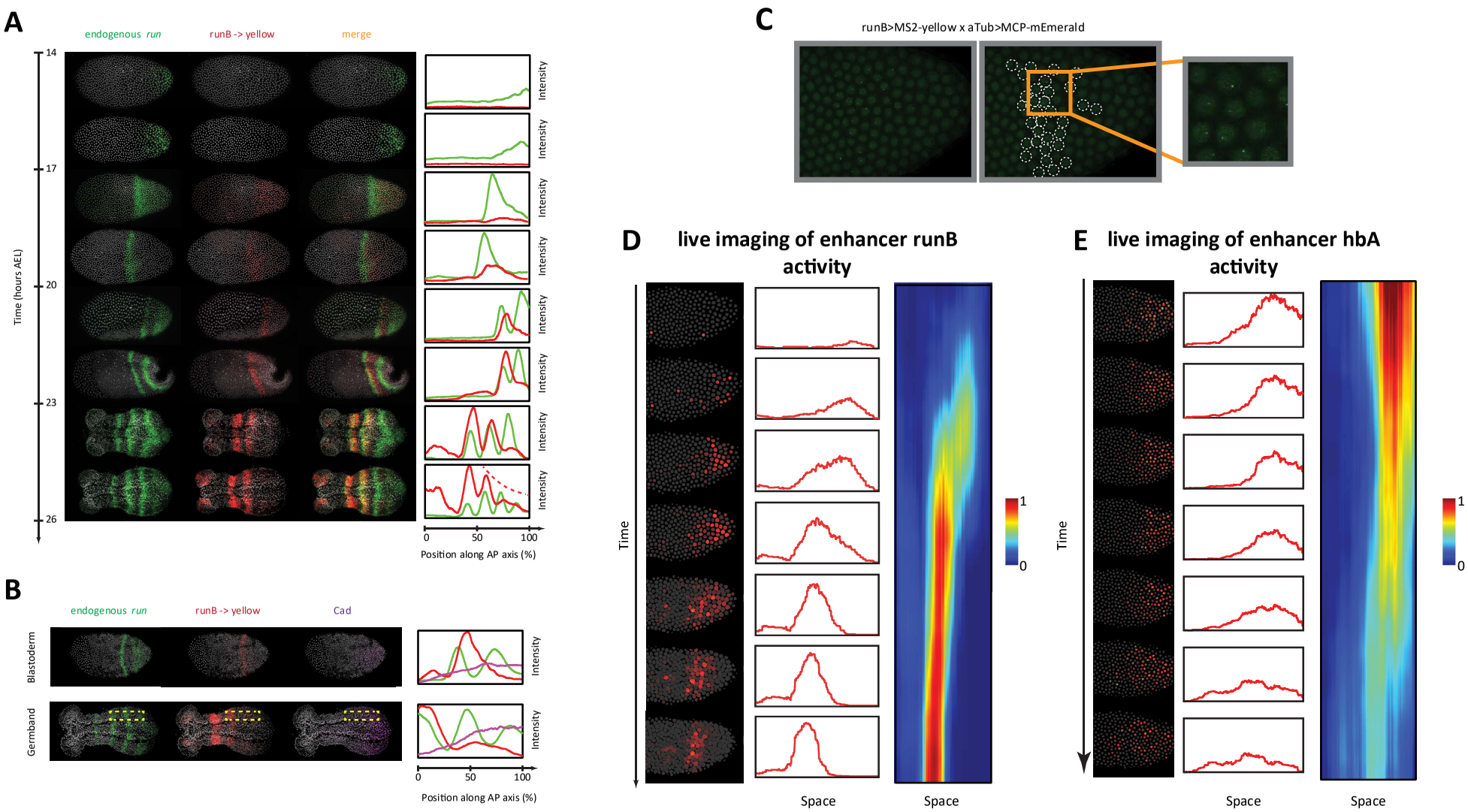


**Figure 6. Analysis of enhancer activity dynamics using the MS2-MCP live imaging system.**

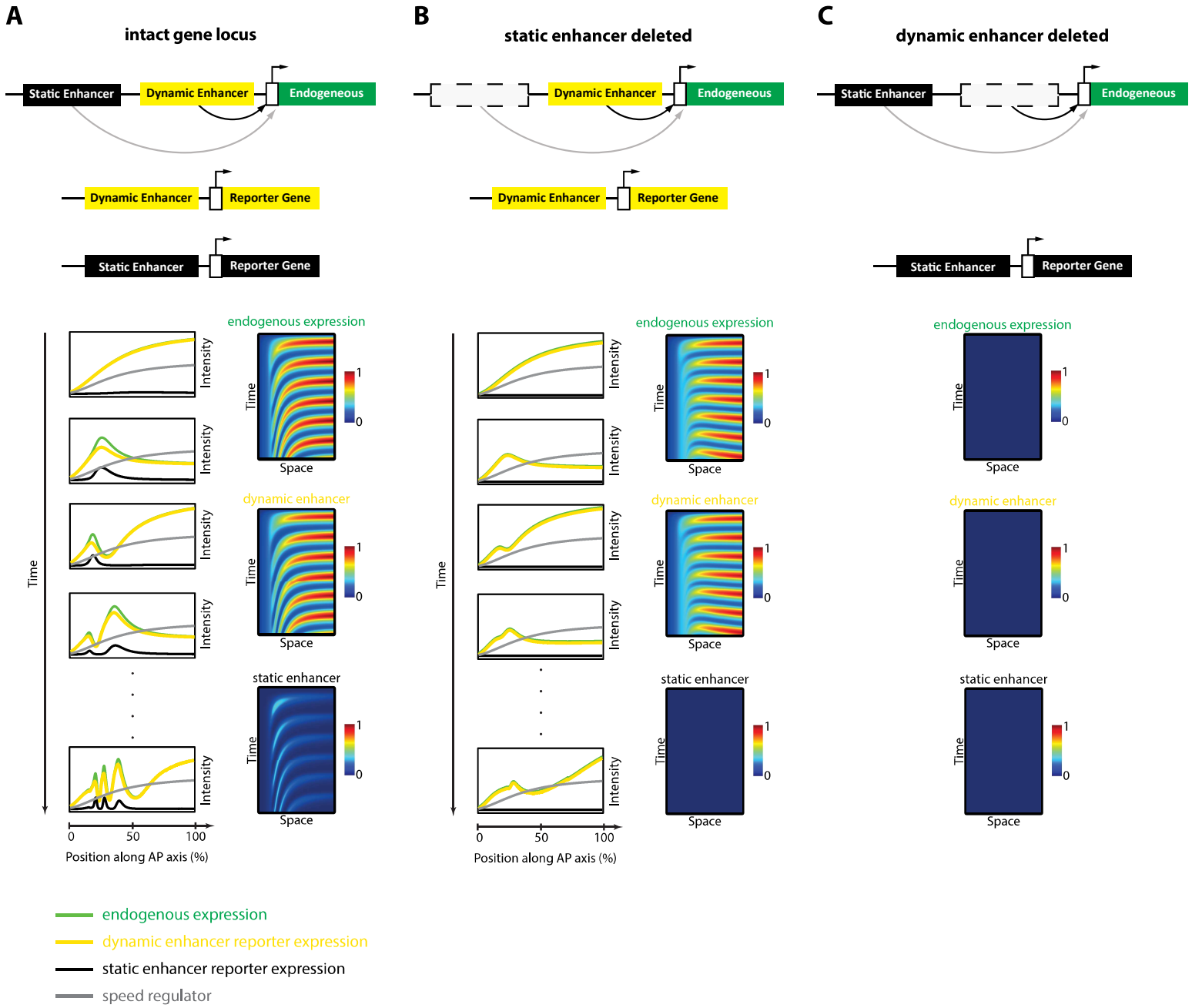


**Figure 7. Simulation of the Enhancer Switching Model with deleted enhancers.**